De-aliasing of Doppler Spectrum for a Fast Scanning Phased Array Radar

Thesis Report

Sultan Abdul Kader

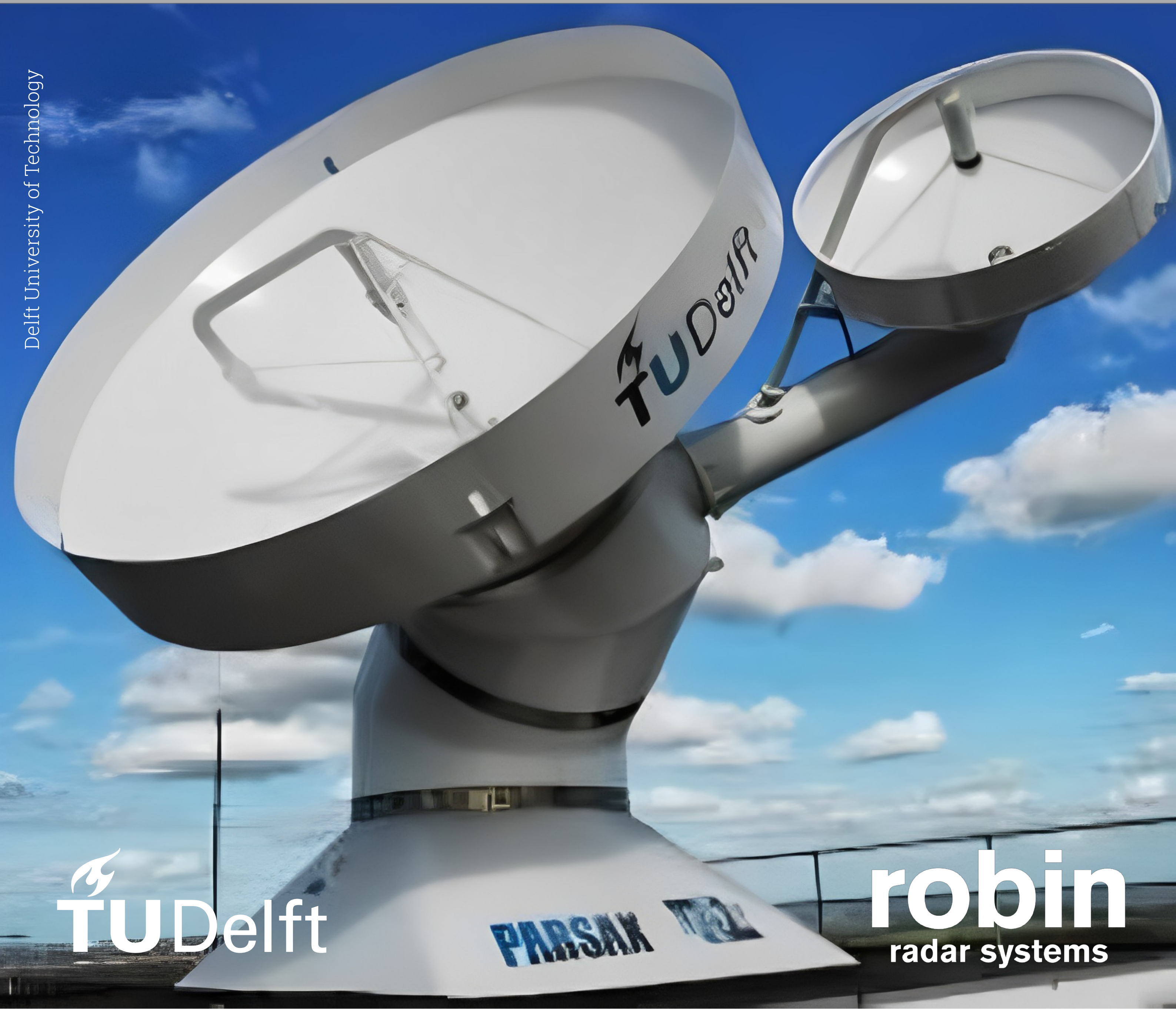

Delft University of Technology

TU Delft

robin
radar systems

De-aliasing of Doppler Spectrum for a Fast Scanning Phased Array Radar

by

Student Name	Student Number
Sultan Abdul Kader Syed Mohamed	5468868

First Supervisor:	Dr. Oleg Krasnov
Daily Supervisor:	Mr. Tworit Dash
Industry Supervisor:	Mr. Jelle Bout
Industry Partner:	Robin Radar Systems
Project Duration:	December, 2022 - August, 2023
Faculty:	Faculty of Electrical Engineering, Delft

Cover: http://radar.ewi.tudelft.nl/Research/project.php?id=80

Acknowledgement

”All praise is due to Allah”

Ladies, gentlemen, and fellow quest seekers,

Today, I stand before you, not as a solitary scholar, but as a mosaic woven together by the threads of support and mentorship.

Prof. Olexander Yarovyi, you’re ’Master Yoda’ to our squad. Your legacy stands as a testament to the heights we can achieve through unwavering dedication and profound wisdom.

Dr. Oleg Krasnov, your mentorship has been a compass pointing me toward scholarly shores, guiding me through the turbulent waves of research with unwavering resolve.

Mr. Tworit Dash, you’re more than a supervisor; you’re the orchestrator of my academic symphony. Your faith in my abilities conducted the melody of success, while your insights were the harmonies that enriched my understanding.

Mr. Jelle Bout, your patient tutelage at Robin Radar Systems was akin to a skilled craftsman shaping raw talent into refined expertise. Your trust in my journey paved the way for growth and mastery.

A heartfelt thank you to Robin Radar Systems for bestowing upon me this incredible opportunity. I’ve relished every moment of it, and I’m grateful for the trust you’ve placed in me. The team has never ceased to inspire, encourage, and support me throughout my journey.

To my friends, you’ve been the oasis of camaraderie in this parched desert of academia. Your jokes have been my water, your encouragement my shade, and your unwavering presence, my compass home. Your insane antics kept me sane.

To my parents, your belief in msy capabilities, even during my moments of doubt, has been the driving force propelling me forward. I have flourished through your words of care and support.

To my brother, whose unwavering support defies time zones and busy schedules. In the midst of his own pursuits, he managed to offer constant care and words of motivation.

As I face this thesis defense, I’m not alone; I’m a constellation of influences, a symphony of support. Each of you has imbued my journey with purpose, turning a solitary academic pursuit into a vibrant adventure.

Here’s to the mentors, friends, and family who have helped me transcend the boundaries of a thesis defense, making it a testament to the collective effort and shared victories. Live long in peace and prosper !!!

Sultan Abdul Kader
Delft, August 2023

Summary

This thesis explores the dealiasing methods of the Doppler spectrum for the case of a fast-scanning weather radar with the possibility of being used in the development of future weather radars. From the literature, log-periodic sampling which is a type of non-uniform sampling is adapted for Doppler dealiasing. The sampling parameters of log-periodic are optimized to provide superior point Doppler dealiasing performance by orders of magnitude. To extend the dealiasing to weather targets with a wider spectrum, the log-periodic sampling is embedded into a 'Periodic Non-Uniform Non-Coherent Burst (PNU-NCB)' structure. Additionally, the unique structure of PNU-NCB enables it to be used readily for fast-scanning radars as a multi-burst processing scheme. Furthermore, an Iterative Adaptive Approach (IAA) algorithm is used in combination with PNU-NCB to suppress the effect of noise and enable the estimation of Doppler moments for wider Doppler targets. The final performance of the designed waveform after processing yields the dealiasing and estimation of moments for even extended Doppler targets with extremely good performance. By using, the optimized PNU-NCB coupled with IAA, it is possible to accurately estimate the Doppler moments unambiguously for targets smaller than 0.1 times the uniform sampling Nyquist window. For higher target spectral width, the estimation of the spectral moments is comparable to the performance in the uniform sampling case with the added benefit of resolving ambiguities. Further performance improvements to the performance can be achieved by exploring the future recommendations provided.

Contents

List of Figures

List of Tables

Nomenclature

Abbreviations

Abbreviation	Definition
FMCW	Frequency Modulated Continuous Wave
CW	Continuous Wave
CPI	Coherent Processing Interval
PRF	Pulse Repetition Frequency
SRF	Sweep Repetition Frequency
FFT	Fast Fourier Transform
DFT	Discrete Fourier Transform
1 ms Nyquist window	Unambiguous velocity (two-sided) in the case of 1 ms uniform sampling
IAA	Iterative Adaptive Approach algorithm
PNU	Periodic Non-Uniform sampling
PNU-NCB	Periodic Non-Uniform sampling with Non-Coherent Bursts

1

Introduction

1.1. Background

Modern radar systems require enhanced capabilities for detecting fast-moving targets that are further away from the radar. However, the presence of aliasing in the signal processing chain may result in ambiguities which lead to false detections or ghost targets. Aliasing is possible in both range and Doppler velocity domains, both are dependent on the Pulse Repetition Frequency (PRF) in the radar hardware system. To increase the extent of the unambiguous limit in one domain, it is required to have a compromise in the other domain and change the radar hardware parameters as well. Limitations in the hardware restrict the maximum unambiguous measurement interval for the case of Doppler velocity processing. In the case of weather radars where there are meteorological targets, aliasing plays a critical role. In such a case, the target response appears extended in both range and Doppler domains. In the Doppler domain, the occupied frequency is a spectrum and thus aliasing might lead to spectral folding or even overlapping of spectra. In the range domain, aliasing leads to false targets and blind-range regions.

Meteorological predictions are done based on the estimated moments (primarily the first two moments - mean and standard deviation) of the spectrum. When such an aliasing effect occurs it is not possible to accurately estimate the spectral moments. This is especially true in the case of a fast-scanning radar, where the time on target is limited which in turn results in a small unambiguous Doppler interval. Doppler spectrum estimation is essential for determining wind speed and turbulence. There have been a few attempts to remove this aliasing effect by using post-processing algorithms or staggered PRF but the performance of these methods is limited and the trade-offs are large.

This thesis aims to remove the aliasing effect by the use of non-uniform sampling methods in the signal processing chain to improve the detection extent and the estimation of target parameters. The use of non-uniform sampling requires a new transmit waveform design and additional steps in processing the received signal but yields promising results. The thesis is done in partnership between TU Delft and Robin Radar Systems.

1.2. Problem statement

In radar systems, the trade-off between unambiguous range and unambiguous velocity is well-known for both pulse and FMCW radars. Increasing the Pulse Repetition Frequency (PRF) or the Sweep Repetition Frequency (SRF) increases the maximum unambiguous velocity that can be measured but

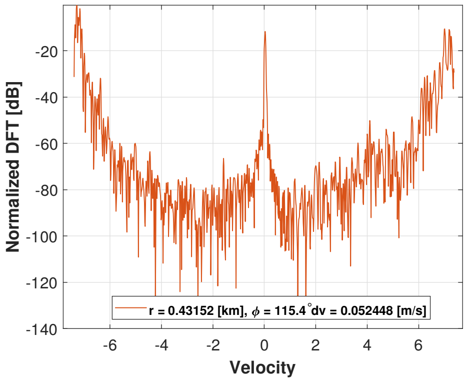

Figure 1.1: Rain event- folded Doppler spectrum

simultaneously decreases the maximum unambiguous range interval. For a fixed PRF/SRF, the maximum unambiguous velocity that can be measured is limited by the maximum phase difference allowed between successive measurements. This is limited by the time spacing between the successive measurements given by the well-known 'Nyquist rate'. The maximum unambiguous velocity for a given value of PRF and operating frequency is given by

$$|v_r^{un}| \leq \frac{\lambda \cdot PRF}{4} \tag{1.1}$$

where v_r^{un} is the maximum unambiguous radial velocity and λ is the operating wavelength of the radar. While the maximum unambiguous range is given by

$$|R_m ax^{un}| \leq \frac{c}{2 \cdot PRF} \tag{1.2}$$

where $R_m ax^{un}$ is the maximum unambiguous range. The FMCW radars have a similar relationship (SRF instead of PRF) with the maximum unambiguous velocity and the maximum unambiguous range.

In order to measure higher unambiguous velocities, it is required to obtain the Doppler measurements in shorter intervals. Hardware limitations or requirements in the maximum unambiguous range usually make faster velocity measurements infeasible. Hence, the need for an alternate approach to extend the maximum unambiguous velocity measurements arises.

When trying to observe the velocities beyond the Nyquist limit, spectral aliasing occurs. Aliasing causes overlapping of the spectra of the grating lobes within the frequency range of observation, as shown in Fig.1.1 for an extended Doppler target case. Here, the target spectrum appears folded and so the Doppler moments estimation will be inaccurate when evaluated over this window.

Estimating the Doppler moments in such a case is incorrect. In order to calculate the proper moments either complex post-processing algorithms or appropriate visual inspection has to be used. These methods are non-ideal and have their own disadvantages.

1.3. State of the art

The problem of mitigating aliasing is a prominent topic of interest in many domains including mixed-signal processing and antenna systems. This has led to the development of several techniques that are addressing specific problems in the respective fields. A few of the state-of-the-art methods of de-aliasing Doppler velocity in radars are given below.

1.3.1. UNRAVEL: post-processing algorithm

The Unfold Radar Velocity (UNRAVEL) stands as an open-source, modular algorithm [1] designed for Doppler velocity de-aliasing within weather radar systems. This innovative solution operates independently of external reference velocity data and encompasses a framework comprising 11 fundamental modules and two distinct de-aliasing strategies. UNRAVEL employs an iterative aplproach, progressively refining parameters to incorporate additional outcomes derived from reference points that have the lowest spectral power. The algorithm further integrates 3D continuity checks into its methodology, and its modular design permits the integration of expanded de-aliasing strategies, facilitating the optimization of outcomes.

Furthermore, Unravel incorporates various techniques to mitigate the impact of absent or corrupted data, thereby addressing issues related to discontinuities. Notably, Unravel consistently demonstrated superior performance in comparison to well-established de-aliasing algorithms, including the 4DD algorithm [2], the unwrap algorithm [3], the region-based algorithm implemented in Py-ART [4], and the multipass algorithm [5].

1.3.2. Staggered PRF

In order to achieve a trade-off between the unambiguous velocity and unambiguous range, multiple bursts of signals are used with each burst alternating in high and low PRF. This approach is called Staggered PRF. The High PRF burst enables larger unambiguous velocities while the low PRF burst determines the unambiguous range. This method combines the advantage of both PRF methods, with increased complexity in the signal processing front.

Unfortunately, the required unambiguous velocity range cannot be met in hardware-limited systems where higher PRF is not possible. Additionally, the staggered PRF introduces multiple artifacts which are detrimental to the detection and estimation of target parameters. These artifacts are shown in Fig.1.2, where the frequency axis is normalized to the unambiguous velocity (two-sided) in the case of 1 ms uniform sampling.

1.3.3. WideBand signals

The narrowband ambiguity function exhibits repetitive ambiguities (grating lobes) for both range and velocity. These repetitive ambiguities are closer and more problematic for a low-PRF pulse train. Conversely, the wideband ambiguity function features a distinct main lobe positioned at the origin, accompanied by multiple responses around ambiguous velocities, known as ambiguous sidelobes (which do not have the same power level as the main lobe). This is due to the presence of a large number of frequency components in the signal which are intrinsically used to eliminate ambiguities.

Consequently, employing a burst of wideband pulses at a low PRF enables the simultaneous unambiguous measurement of unambiguous target range and velocity within a single CPI (Coherent Processing Interval) [6]. Notably, the ambiguous sidelobes with typical wideband burst parameters, maintain a level between -20 dB and -5 dB as shown in Fig.1.3. Such elevated sidelobe levels are generally unsuitable for surveillance radars that aim to detect weak targets amidst strong clutter. In such cases, the sidelobe level required by typical surveillance radars is -30 dB or lower.

There are several algorithms that exploit the unique structure of the wideband ambiguity function (where the main lobe is the highest peak) to aid in target detection, one of them is discussed in detail in chapter 5. Ultimately, this approach requires the transmitted waveform and the processing chain to be able to process larger bandwidth signals, which is expensive and induces complexities.

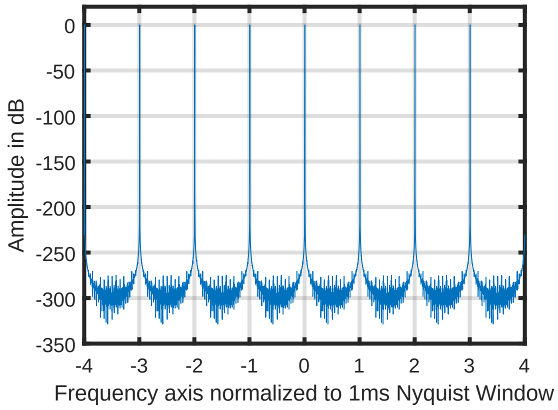

(a)

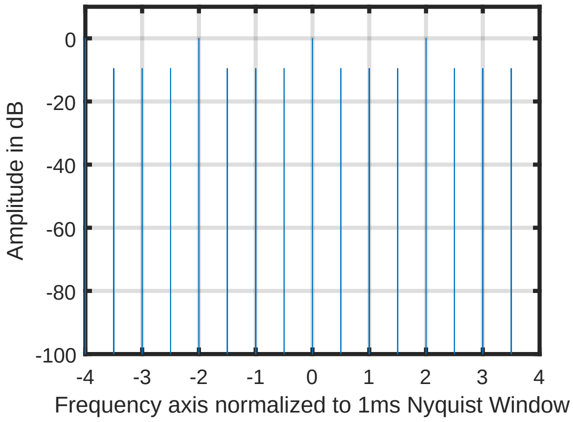

(b)

Figure 1.2: Uniform PRF vs Staggered PRF: a) Uniform PRF case ; b) 2-burst Staggered PRF with lower number of ambiguous grating lobes (amplitude equal to target's main lobe) but higher sidelobe levels (artifacts created due to suppression) ;

1.3.4. Non-uniform sampling

In power spectral evaluation, it is well-known that the aliasing effect occurs when the frequency of observation is higher than half of the sampling frequency. This is denoted by the famous Nyquist sampling rate given by:

$$f_m \leq f_s/2 \tag{1.3}$$

where f_m is the maximum frequency of the message signal that can be observed without aliasing and f_s is the sampling frequency.

In the uniform sampling scenario, the sampling time (or the sampling frequency) is constant and so the Nyquist limit is fixed. But for the non-uniform sampling case, the Nyquist limit is not well-known. More information on the non-uniform sampling Nyquist limit is discussed in section 2.2. Nevertheless, the potential of non-uniform sampling to remove grating lobes has been explored in various other domains such as antenna systems and data converters.

A specific type of non-uniform sampling for the case of de-aliasing has been discussed in [7] called log-periodic sampling. Here the spacing between the samples is based on an exponential curve. The sampling time between each of the signal points in the time domain is given by

$$g(z) = (T/N)(b/a)\left[e^{az} - 1\right] \tag{1.4}$$

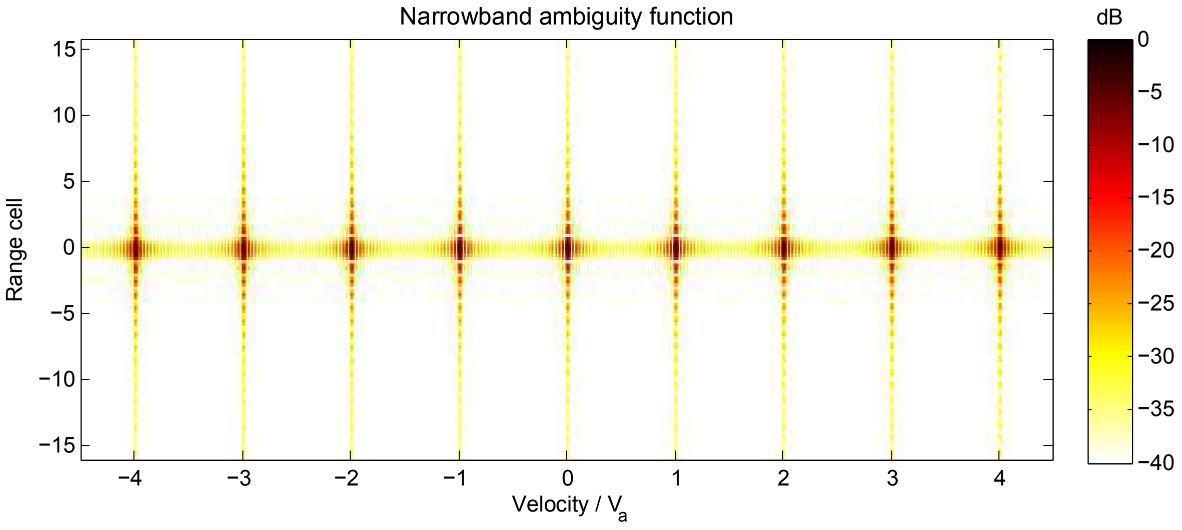

(a)

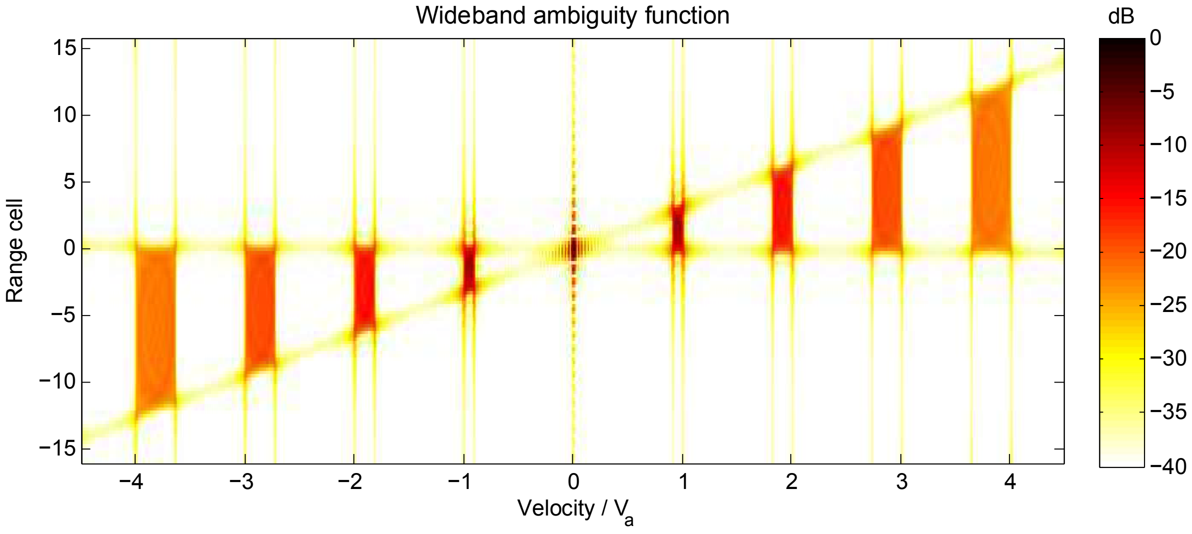

(b)

Figure 1.3: Narrowband vs Wideband ambiguity function: a) Narrowband ambiguity function with grating lobes of equal amplitude to the main lobe ; b) Wideband ambiguity function with ambiguous sidelobes of lower amplitude ;

where z is the discrete sample index, N is the number of Doppler samples within a burst, T is the total measurement duration (which is equivalent to the CPI of the entire bursts), b is the initial minimum sample spacing, and a is the exponential growth rate of the sample time increments.

In addition, a Hanning window taper function is applied to the entire spread of data to minimize the unwanted artifacts arising due to spectral leakage. The Hanning window is the most widely used windowing function which gives good frequency resolution and is applicable for random signals with less distortion in the amplitude of the signal. The comparison of the uniform sampling vs the log-periodic spacing for values of $b = 0.5$ and $a = 0.001228$ is shown in Fig.1.4.

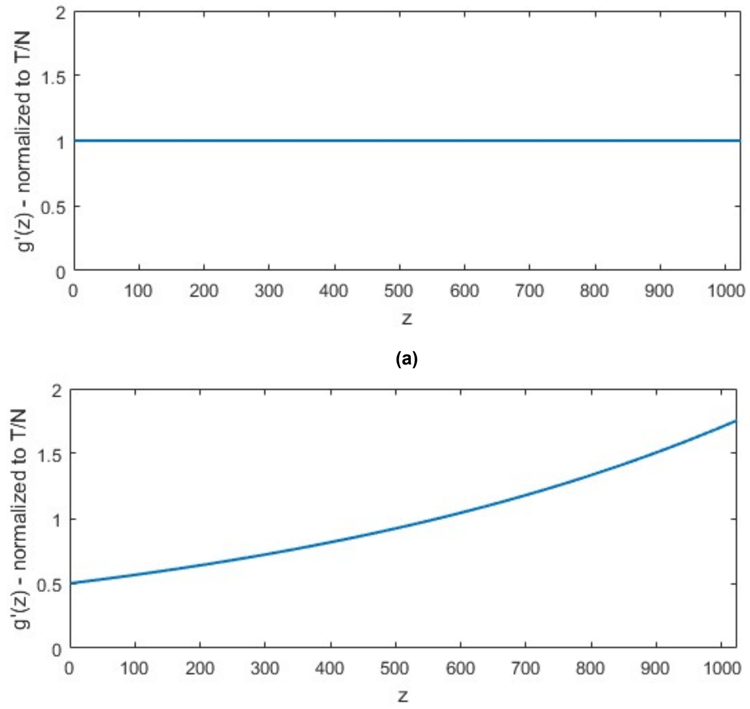

(a)

(b)

Figure 1.4: Sample time difference for sampling strategies a) Uniform sampling case ; b) log-periodic sampling case where the samples are spaced along an exponential curve

From the literature, the non-uniform sampling strategy is capable of resolving ambiguities in the case of point targets. But the extent of the Nyquist limit and the performance for extended targets has not been explored fully. The drawbacks associated with this method would be the placement of the transmit signal samples at precise time stamps and the complicated signal processing involved at the receiver.

1.4. Research objectives

From the literature, it is evident that the current methods for de-aliasing hold some drawbacks. The following research gaps needs were found in the literature review of this thesis:

- Specifically, the UNRAVEL algorithm mentioned in subsection 1.3.1 is a post-processing algorithm, it is inherently better to find a pre-processing method that can de-alias the signal. Moreover, the unwanted artifacts and noise level after processing should be minimum to ensure proper detection performance.
- The log-periodic sampling method stated in subsection 1.3.4 seems to have very good potential in achieving de-aliasing but other types of non-uniform sampling have yet to be explored and their performance with respect to the radar Doppler scenario is yet to be verified.
- Additionally, all the previous literature has considered the possibility of de-aliasing a point target only but in the case of meteorological targets, it is necessary to consider targets that are extended in the Doppler domain.

The goal of this thesis is to remove the Doppler aliasing (grating lobes) or enhance the unambiguous Doppler velocity interval without any compromise in the unambiguous range interval. Primarily, by using non-uniform sampling for extended targets and in the presence of noise.

1.5. Novelties in this thesis

The list below encompasses the contributions and novel aspects incorporated to accomplish the research objective of this thesis:

- The representation of non-uniform sampled signals promoted a challenge since the MATLAB Fast Fourier Transform (FFT) function only works with uniform time samples. Other non-uniform visualization methods such as Lomb-Scargle periodogram, were computationally expensive. By using an extended time axis of finer step size to position the non-uniform pulses/sweeps, it was made possible to use the Discrete Fourier Transform (DFT). This enables easier power spectrum calculation saving considerable time without compromising performance.
- The non-uniform sampling procedures in literature have considered only point targets. For, extended targets only post-processing works were done. This thesis formulated the non-uniform sampling for extended Doppler targets and has successfully de-aliased the spectrum. Additionally, the capability of non-uniform sampling to detect multiple extended targets has also been explored and proven successfully.
- In order to get higher SNR, the structure of the log-periodic sampling spectrum (a type of non-uniform sampling discussed in chapter 3 is exploited by using the Iterative Adaptive Approach (IAA) algorithm, which is a parameter-free data-adaptive noise suppression algorithm. The algorithm's application in the non-uniform sampling scenario is unprecedented, and its performance has proven to be exceptional.

1.6. Thesis roadmap

This thesis starts by exploring the various state-of-the-art techniques and their performance on the de-aliasing front. The comparison of the performances of de-aliasing strategies of UNRAVEL algorithm, staggered PRF, wide-band signal, and non-uniform sampling is done. Non-uniform sampling is chosen as the primary approach since it is relatively unexplored and has superior performance to the others. Then, the Non-Uniform sampling theory, its limitations, and de-aliasing performance are analyzed in chapter 2. The spectral calculations for non-uniform sampling are an additional challenge that needed to be solved. A comparison of the spectral estimation methods for the non-uniform sampling is also done.

In the context of non-uniform sampling, many approaches were available and of those, two strategies have been chosen for implementation- 'log-periodic sampling' and 'periodic non-uniform sampling' is discussed in chapter 3 and chapter 4. The target modeling, the performance of the methods, and their parameter dependencies are discussed as well. The performance of the non-uniform sampling in the presence of noise is found to be enhanced by the novel use of the Iterative Adaptive Approach (IAA) algorithm which is discussed in chapter 5. The focus is primarily on successful detection without ambiguities and then accurately estimating the target's spectral moments.

In chapter 6, the performance of the suggested approaches was verified theoretically using a Monte-Carlo simulation of 100 trials for different noise levels, different target spectral widths, and waveform parameters. Experimental verification of the results was also done with the PARSAX radar in TU Delft which shows excellent performance. Finally, the conclusions and the recommendations for future work are discussed in chapter 7.

Chapter References

[1] V. Louf et al. “Unravel: A robust modular velocity dealiasing technique for doppler radar”. In: *Journal of Atmospheric and Oceanic Technology* 37.5 (May 2020), pp. 741–758. DOI: `10.1175/JTECH-D-19-0020.1`.

[2] C. N. James and R. A. Houze. “A Real-Time Four-Dimensional Doppler Dealiasing Scheme”. In: *Journal of Atmospheric and Oceanic Technology* 18.10 (2001), pp. 1674–1683. DOI: `https://doi.org/10.1175/1520-0426(2001)018<1674:ARTFDD>2.0.CO;2`.

[3] D. R. Burton et al. “Fast two-dimensional phase-unwrapping algorithm based on sorting by reliability following a noncontinuous path”. In: *Applied Optics, Vol. 41, Issue 35, pp. 7437-7444* 41.35 (Dec. 2002), pp. 7437–7444. DOI: `10.1364/AO.41.007437`.

[4] J. J. Helmus and S. M. Collis. “The Python ARM Radar Toolkit (Py-ART), a Library for Working with Weather Radar Data in the Python Programming Language”. In: *Journal of Open Research Software* 4.1 (July 2016), p. 25. DOI: `10.5334/jors.119`.

[5] J. Zhang and S. Wang. “An Automated 2D Multipass Doppler Radar Velocity Dealiasing Scheme”. In: *Journal of Atmospheric and Oceanic Technology* 23.9 (2006), pp. 1239–1248. DOI: `https://doi.org/10.1175/JTECH1910.1`.

[6] N. Petrov. “Migrating Target Detection in Wideband Radars”. In: *TU Delft Repositories* (). DOI: `10.4233/uuid:08556a7c-ef90-43f7-998b-f103ceea6267`.

[7] A. W. Doerry. *Radar Doppler processing with nonuniform PRF*. Tech. rep. 2017. DOI: `10.2172/1373645`.

2

Non-Uniform Spectral Characterization

2.1. Problem Formulation

In contrast to the well-established uniform spectral characteristics, the non-uniform sampling spectrum has certain unique characteristics. For uniform sampling, the maximum observable frequency is defined by its sampling time. However, for non-uniform sampling, the maximum observable frequency can go beyond this limit. Additionally, there is a lot of confusion and misinterpretation associated with the Nyquist limit for non-uniform sampling [8][9]. Furthermore, visualization of the spectrum of unevenly sampled signals cannot be done by using traditional methods without some modifications. There are certain spectral calculation methods that are designed explicitly for non-uniform sampling. The non-uniform Nyquist limit, the spectral calculation, and the dependencies for such non-uniform sampling are discussed in this chapter.

2.2. Nyquist limit for non-uniform sampling

In the uniform sampling case, the Nyquist limit is well-defined and is given by (1.3). In the case of non-uniform sampling, the existence of the ”Nyquist limit” is debated and is uncertain in most of the literature. Even if it does exist, it typically holds lesser significance than the ’uniform sampling Nyquist limit’ due to its immensely larger value [9].

For the non-uniform sampling, there is a Nyquist limit as mentioned in [8] which is governed by the time difference between the samples. This is given by the equation shown below,

$$t_i = t_0 + n_i p \tag{2.1}$$

where t_0 is the first sample time, t_i is the i^{th} sample time, and p is the greatest common factor among all the time differences between successive echos such that each time difference Δt_i is an exact integer multiple (n_i) of p. In order to determine the Nyquist limit for non-uniform sampling, one must identify the greatest factor p that satisfies (2.2). Thus the non-uniform Nyquist limit is then given by

$$f_{\text{Nyq}} = \frac{1}{2p} \tag{2.2}$$

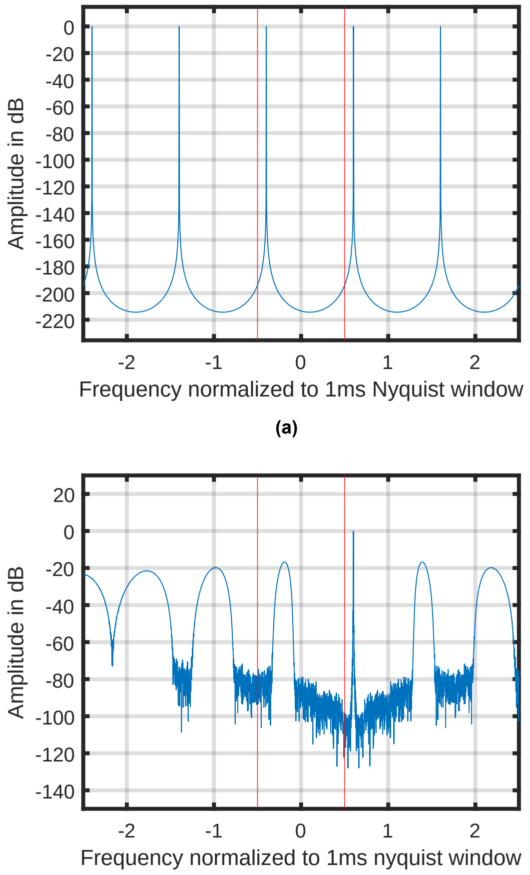

Figure 2.1: Comparison of Nyquist limits for uniform and non-uniform case. a) Uniform sampling case with aliasing- sampling time is 1ms and 5 times the 1ms Nyquist window is shown with the target at 600 Hz. The original Nyquist window is shown within the red vertical lines. b) Non-Uniform sampling case with 1 μs timestamp accuracy- The actual target is found in this case without aliasing.

where f_{Nyq} is the maximum frequency that can be observed using non-uniform sampling. This definition of the maximum observable frequency also holds true for uniform sampling case as in (1.3), where p is equal to the uniform sample spacing (which is equivalent to the inverse of f_s).

2.2.1. Special case: Irrational sample spacing

There exists a special case when the spacing between the samples is irrational. In such a scenario, there is no common factor p between the sample spacing; thus, there is no Nyquist limit. Unfortunately, this holds true only for an ideal case where the time samples can be measured with infinite precision. For a real-life system that only records the time stamp of samples accurately to D decimal places, a more realistic Nyquist limit exists given by,

$$f_{\text{Ny}} \leqslant \frac{1}{2} 10^D \tag{2.3}$$

Intuitively, if the radar is only capable of measuring received echo with 1 micro-second precision, then the largest common factor between irrational samples would be 1 micro-second. Thus for the irrational sampling space case, (2.2) and (2.3) are essentially the same.

A comparison of the aliasing effects for the case of uniform sampling and the case of non-uniform sampling is given in Fig.2.1. In both Fig.2.1a and Fig.2.1b, the minimum spacing between samples

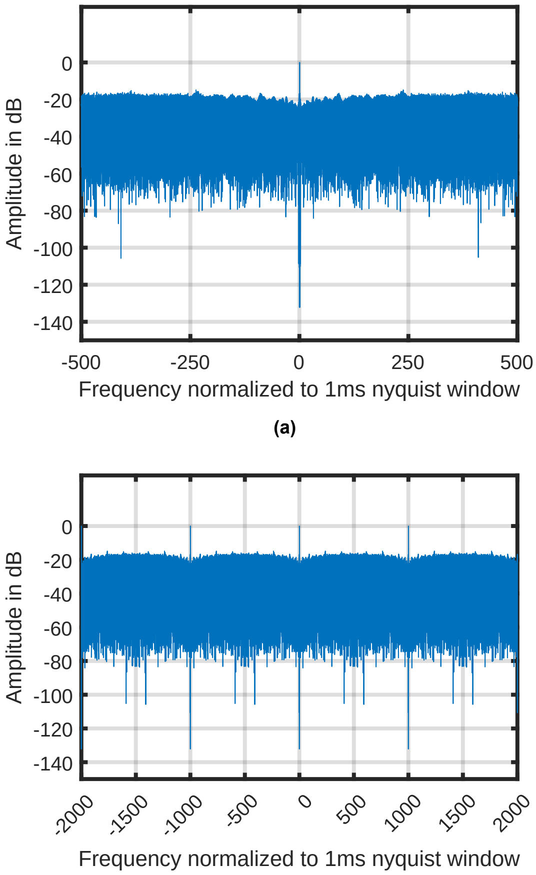

(a)

(b)

Figure 2.2: Nyquist limit and aliasing for the non-uniform case a) Non-Uniform sampling case with 1 μs timestamp accuracy- full unambiguous non-uniform Nyquist interval which is 1000 times the 1 ms uniform Nyquist interval. b) Non-Uniform sampling case with aliasing- frequency of observations is 3 times the unambiguous 'non-uniform Nyquist interval'.

is maintained to be 1 millisecond. Fig.2.1a shows the aliasing effects when the frequency of observation goes beyond the traditional uniform Nyquist window. For simpler analysis, the frequency axis is normalized by the 'unambiguous (two-sided) frequency interval in the case of 1 ms uniform sampling' throughout this thesis. Therefore, a normalized frequency range from -0.5 to 0.5 is equivalent to -500 Hz to 500 Hz. It can be clearly seen that when a point target is present at the frequency of 600 Hz (0.6 in the 1 ms Nyquist window normalized frequency axis), it is aliased and an ambiguous target is found at the frequency of -400 Hz (-0.4 in the normalized frequency axis).

In the case of non-uniform sampling as shown in Fig.2.1b, the ambiguous targets are reduced to ambiguous sidelobes with lower sidelobe levels, hence the target can now be clearly distinguished. In Fig.2.2a, the full extent of the non-uniform Nyquist window for log-periodic sampling (a type of non-uniform sampling discussed in chapter 3) with 1 micro-second steps is shown. It can be seen that the unambiguous limit is 1000 times the 1 ms Nyquist window of the uniform sampling case. Meanwhile, Fig.2.2b shows that the power spectrum beyond the non-uniform Nyquist limit where the aliased target can be seen.

2.3. Non-Uniform signal parameters

In order to compare the performance of non-uniform sampling (with the uniform sampling case), the signal parameters in this thesis project are made to adhere to a specific standard such that the comparison is justifiable. A uniformly sampled signal with a constant sampling time of 1 millisecond is considered to be the reference signal. This translated to a Nyquist frequency limit of -500 to 500 Hz (-0.5 to 0.5 times the frequency normalized to $1ms$ Nyquist window) in accordance with (1.3). This is the unambiguous frequency limit window that is to be improved. Beyond this window, the uniformly sampled spectrum is just the aliased replica of the original spectrum present within the window.

For the non-uniform sampled scenario, the spacing between the radar echo samples in time is ensured to be at least 1 millisecond as in the uniform sampling case. This guarantees that the increase in the unambiguous interval is not just because the samples are closer together without any effect of non-uniform sampling. Furthermore, the hardware clock frequency in current radars is well above the 1 MHz range which enables placement of the samples with 1 μs precision. In conclusion, the placement of non-uniform echo samples in time depends on two factors:

- A minimum spacing of 1 millisecond is required between the samples,
- The samples can be placed in steps of 1 micro-second in the time axis as long as they satisfy the minimum spacing criteria.

All the experiments done for this thesis ensure that the transmitted waveform samples satisfy these two criteria. Thus, the results are purely an effect of non-uniform sample spacing and the parameters associated with it.

2.4. Calculation of Non-uniform sampled spectrum

The spectral calculation for non-uniformly sampled data has been extensively used in astronomy where the signals from certain celestial bodies are spare in nature [10] and can only be obtained when all the favorable measurement conditions are met. Additionally, for non-uniform sampling, the power spectrum calculation is done using the MATLAB FFT algorithm by making novel changes to the input.

In conclusion, power spectral calculation is done by the following three methods, which are elaborated below:

1. In-built MATLAB FFT Algorithm
2. Lomb-Scargle Periodogram
3. DFT equation-based estimation

2.4.1. In-built MATLAB FFT Algorithm

Historically, the Fast Fourier Transform (FFT) algorithm in MATLAB was primarily intended for uniform sample data. It offers advantages such as computational efficiency and excellent performance. Using the FFT algorithm could offer better insights into the spectral analysis of non-uniformly sampled signals.

The modeling of FFT to incorporate non-uniform samples is one of the main novelties done in this thesis. For the uniform sampling case, the samples were in 1-millisecond intervals (the sample times in milli-seconds would be 1,2,3,...) thus, for a Coherent Processing Interval (CPI) of 0.8 seconds, the number of samples is 800.

But for non-uniform sampling, the samples are positioned at micro-second intervals (a typical example of non-uniform sample time in milliseconds is 1.008,2.05,3.132,...) thus the use of a millisecond time axis becomes invalid. Thereby for non-uniform sampling, a microsecond time axis is used. Implying that for the same Coherent Processing Interval (CPI) of 0.8 seconds, there will be 800,000 possible locations in the time axis. The transmitted waveform is designed such that the pulses/sweeps start at the chosen non-uniform time instances. From the respective received burst, we place the Doppler radar echo samples at the respective locations in the 800,000 possible positions. All the other sample values are made to be equal to zeros.

For example, if the sample times are 1.008 ms and 2.050 ms then the first pulse will be sent at 1008^{th} micro-second and the second pulse will be sent at 2050^{th} micro-second. The time axis has uniform micro-second spacing and the signal input to FFT has the corresponding 1008^{th} and 2050^{th} sample values from the received pulses while all the other signal values in between are made to be zero.

The drawback of this method is that the representation of the signal in terms of the number of samples and calculation of the spectrum increases by a factor of 1000 (equivalent to the ratio of 1 milli-second to 1 micro-second). But since most of the samples are zeros it reduces the computational complexity. Additionally, since the samples are spaced with a minimum spacing of 1 millisecond, the total number of valid samples (non-zero samples) will be lesser than the number of samples in the uniform case (less than 800). This might increase the sidelobe levels in the spectrum to some extent but does not impede any crucial aspect of signal processing. An algorithm to increase the SNR and mitigate the effect of sidelobes is discussed in chapter 5. Adding multiple zeros to the original sampling space is similar to zero-padding, a common signal-processing technique to get a smoother spectrum and reduced side lobes. Similarly, the disadvantage of zero-padding also applies here namely, increased computational complexity and smoothing of the spectral graph. An analysis of the frequency resolution of the target is done in subsection 2.4.4.

2.4.2. Lomb-Scargle algorithm

One of the prominent methods used in astronomical non-uniform signal processing is the Lomb-Scargle algorithm [11] [12] which is a least-squares spectral estimation method. It is specifically designed for analyzing periodicity in time series with uneven sampling intervals. This method is more computationally expensive compared to the Fourier transform approach. Furthermore, The algorithm is sensitive to outliers such as a noise spike in the time domain or sampling inaccuracies. This results in a bias and may ultimately lead to inaccurate results even if only one of the data points is invalid or erroneous.

Furthermore, the frequency resolution of the Lomb-Scargle periodogram is determined by the length of the time series and the distribution of the data points within it. Thus, the frequency resolution of the Lomb-Scargle periodogram varies based on the specific data set being analyzed. The Lomb-Scargle method adapts and estimates the power spectral density at different frequencies based on the distribution of data points in the time series. Thus, it does not provide a fixed ”binning” of frequency resolution like the traditional Fourier-based methods. Hence, a guaranteed resolution cannot be identified.

2.4.3. DFT equation-based estimation

The most common method of spectral estimation for a discrete representation of the signal is the Discrete Fourier Transform (DFT) method. The DFT spectral calculation is given by,

$$X(k) = \sum_{n=0}^{N-1} x(n) e^{-j2\pi kn/N}, \tag{2.4}$$

where k is the frequency bin for which the spectrum is to be calculated, n denotes the index of the signal samples and N is the total number of samples in the non-uniform sampling scenario (which is less than 800 for a CPI of 0.8 seconds). Since the DFT equation requires the signal samples directly, there is no need for having samples with zero values between two successive valid non-uniform samples. Only the valid samples in 1-microsecond signal representation are considered (i.e. it is enough to give the 1008^{th} sample, 2050^{th} sample, and so on directly as mentioned in subsection 2.4.1). This can be verified since all the other sample values are zero, they do not contribute anything to the spectral calculation. As a result, the calculation of the DFT is less computationally complex and the calculation speed is comparable to the FFT algorithm.

2.4.4. Resolution for Non-uniform sampling

The resolution of a radar refers to its ability to distinguish between closely spaced targets. Specifically, Doppler velocity resolution pertains to the radar's ability to distinguish between targets moving at slightly different velocities. An experimental comparison is done to analyze the resolution of all the methods, there are two reasons why this is done:

- To compare the resolution performance of the different power spectral density calculation approaches.
- To identify if the non-uniform sampling changes the resolution performance (since the number of valid samples is lesser) when compared with the uniform sampling.

There are limitations to the resolution capabilities of the different approaches. Some insights on the limitations of the different approaches are given below:

True frequency present in the signal: For rigid targets, the entire target body moves with the same velocity thus its Doppler frequency is represented by a single frequency bin in the power spectral density. But for meteorological targets, some of the particles in a cloud target may move with a slightly different velocity from the rest of the cloud, and hence the target Doppler velocity is more widespread over a range of spectral bins. In order to know fully the constituents of the signal, the spectral estimation method should ideally have infinite precision.

Frequency resolution of Fourier Transform: This denotes the ability of the Fourier transform to distinguish closely spaced signals at the specific frequencies (frequency bins). The Fourier transform resolution is governed by the length of the time window of measurement or the duration of the signal being analyzed as shown:

$$\Delta f_{\text{sig}} = \frac{1}{T}. \tag{2.5}$$

Thus, the resolution of the Fourier transform can be improved by increasing the total duration (CPI) of the signal. Similarly, for the non-uniform sampling case, the resolution depends on the CPI which is equivalent to the time instance of the last sample. Thus, to maintain the same level of resolution in the experiments and simulations done, the last sample time is always fixed to be close to 0.8 seconds.

Additionally, windowing techniques can help improve the resolution by reducing spectral leakage effects. A Hanning window with a size equivalent to the signal duration is employed throughout this project.

Frequency resolution of Lomb-Scargle periodogram: The frequency resolution of the Lomb-Scargle periodogram is primarily influenced by the length of the time series and the density of the sampling points. Generally, a longer time series with more densely spaced samples will result in higher frequency resolution than the Fourier transform case for unevenly sampled data [9]. As mentioned before, the Lomb-Scargle periodogram does not provide a fixed ”binning” of frequency resolution like the traditional Fourier-based methods.

A comparison between the different spectral estimation methods is shown in the table below:

Method	Computational time	Signal manipulations	Frequency resolution
MATLAB FFT	Low	Modified time axis + Unnecessary computations	Constant
Lomb-Scargle Algorithm	High	Not needed	Unreliable
DFT	Medium	Not needed	Constant

Table 2.1: Comparison of the different non-uniform spectral estimation methods

2.5. Conclusion

In essence, the Nyquist limit for the non-uniform sampling case is different from the uniform sampling case. It is governed by the highest common factor between the sample times if any, as mentioned in (2.2). In the case of irrational sample spacings, the Nyquist limit follows the value of the least significant digit in the time stamp of measurements as stated in (2.3). For the sake of comparison, the 1 millisecond constant sampling time is taken over the entire CPI duration of 800 milliseconds, this denotes the unambiguous interval of -500 Hz to 500 Hz in the uniform sampling case.

As for the non-uniform case, the samples are maintained to have a minimum spacing of 1 millisecond to ensure that the Nyquist frequency window is comparable to the uniform sampling case. Additionally, the consecutive samples are placed in locations with the least significant digit as 1 microsecond yielding an unambiguous interval of -500 KHz to 500 KHz, which is a thousand times the limit for the uniform case. Due to the additional delay beyond the 1-millisecond minimum spacing, the total number of samples in the non-uniform case is lesser than in the uniform sampling case. However, if the last sample timing is the same as the case of uniform sampling CPI then the frequency resolution remains unchanged for both the uniform sampling and the non-uniform sampling case.

Additionally, the calculation of the power spectrum of the non-uniform sampled signal posed a challenge, with the most commonly used method being the Lomb-Scargle algorithm. Since the Lomb-Scargle algorithm is sensitive to outliers and was computationally expensive, alternatives were found. Using the FFT method as mentioned in subsection 2.4.1 requires additional computation but yields an extended frequency spectrum that is far beyond the Doppler frequency range of meteorological targets. Alternatively, the DFT implementation of spectral calculation can be done using the non-uniform samples without any modification to the time axis and the signal. The DFT method also can be used to observe frequencies far beyond the $1ms$ Nyquist interval of the uniform sampling case.

Chapter References

[8] L. Eyer and P. Bartholdi. “Variable stars: Which Nyquist frequency?” In: *Astronomy and Astrophysics Supplement Series* 135.1 (Feb. 1999), pp. 1–3. DOI: `10.1051/AAS:1999102`.

[9] J. T. VanderPlas. “Understanding the Lomb–Scargle Periodogram”. In: *The Astrophysical Journal Supplement Series* 236.1 (May 2018), p. 16. DOI: `10.3847/1538-4365/aab766`.

[10] M. D. Migliore. “On the sampling of the electromagnetic field radiated by sparse sources”. In: *IEEE Transactions on Antennas and Propagation* 63.2 (Feb. 2015), pp. 553–564. DOI: `10.1109/TAP.2014.2379911`.

[11] N. R. Lomb. *Least-squares frequency analysis of unequally spaced data*. Tech. rep. 1976.

[12] J. D. Scargle. “Studies in astronomical time series analysis. II - Statistical aspects of spectral analysis of unevenly spaced data”. In: *The Astrophysical Journal* 263 (Dec. 1982), p. 835. DOI: `10.1086/160554`.

3

Log-Periodic Sampling

3.1. Introduction

In the previous chapter, non-uniform sampling is identified to be superior to uniform sampling in terms of the maximum observable frequency [8] [9]. The next step is to identify a particular non-uniform sampling technique and to study its performance. There are numerous types of non-uniform sampling such as staggered sampling, linearly increasing chirp sampling, random sampling, Gaussian sampling, sinusoidal sampling, log-periodic sampling, etc [13] [14]. According to the literature, log-periodic sampling is the best-performing method [7] regarding low ambiguous sidelobe levels and smooth spectra. Thus log-periodic sampling is chosen in this thesis as the main sampling strategy and its performance is explored.

In this chapter, the target model including the additive noise model used in evaluating the non-uniform sampling is explained. The log-periodic sampling model and its associated parameters are mentioned. Followed by a section on the dependence of the power spectrum on these parameters. Additionally, some insights on the interdependence of these parameters and how to choose the optimum value of these parameters are discussed. The performance of the log-periodic sampling for the case of point Doppler targets and extended targets is discussed. Furthermore, the structure of the ambiguous sidelobes in the log-periodic sampling case is discussed. Finally, log-periodic sampling is tested on extended targets and the results are discussed as well.

3.2. Target Modelling

A target simulation model is developed to analyze the performance of log-periodic sampling. The modeling is based on [15]. The targets are complex with either positive or negative Doppler frequency meaning that the target moves toward or away from the radar. The resulting signal is a complex exponential signal having the mean Doppler velocity, and the Doppler spectrum width as input parameters. The initial phase of the signal is uniformly distributed between [-π,π]. The resulting signal model is given by,

$$s(t) = \sum_{m=1}^{M} a_m e^{j(2\pi f_m t + \beta_m)} \tag{3.1}$$

where

$$a_m = a \quad \forall m$$

Here, $a_m = a = 1$ (i.e. same amplitude for all scatterers). The Doppler frequencies f_m of all the scatterers are assumed to be *i.i.d* Gaussian distributed random variables with mean Doppler frequency μ and variance (the square of the Doppler frequency width) σ^2. Also the initial phase of the signal β_m is uniformly distributed between [-π,π]. The distributions for both the target frequency and target phase are given by,

$$\{f_m\}_{m=1}^{M} \overset{i.i.d.}{\sim} \mathcal{N}\left(\mu, \sigma^2\right)$$
$$\{\beta_m\}_{m=1}^{M} \overset{i.i.d.}{\sim} \mathcal{U}[-\pi, \pi]$$

For the case of point targets, the Doppler spectrum width is taken as zero, and hence even if the target is composed of multiple scattering points it is modeled such that all these points move with the same velocity. For the case of extended meteorological targets, the maximum target standard deviation is found to be 7.5 m/s in velocity which translates to 150 Hz for a 3 GHz radar center frequency. Thus, targets with a Doppler standard deviation of $\frac{1}{40}^{th}$, $\frac{1}{20}^{th}$, $\frac{1}{10}^{th}$, and $\frac{1}{5}^{th}$ the 1 milli-second Nyquist window are used to test the performance. It is to be noted that the typical Doppler standard deviation [16] for meteorological targets is $\frac{1}{20}^{th}$ and $\frac{1}{30}^{th}$ times the size of the 1 ms Nyquist window.

3.2.1. Additive Noise Modelling

Noise is added to the signal to ensure that the algorithms used are valid and can be applied to real-life scenarios. The noise added is a complex white Gaussian noise model. The measurement model in time consists of the signal model and an additive white complex Gaussian noise with variance σ_n^2. The overall measurement vector is given by,

$$\mathbf{z} = \mathbf{s} + \mathbf{n}, \quad with \quad \{n_t\}_{t=0}^{T} \overset{i.i.d.}{\sim} \mathcal{CN}(0, \sigma_n^2). \tag{3.2}$$

where t denotes the time instance where we have the samples, T is the total CPI, and **n** is the vector containing all the values of n_t. For simulation purposes, the noise variance is computed with an user-defined SNR value given as input [15].

3.3. Sampling parameters – N,b,a

In log-periodic sampling, the sample time increments change with each pulse in an exponential manner, i.e. the log of the sample spacing is periodic. The sample time increments are given by,

$$g'(z) = (T/N)\left[be^{az}\right], \tag{3.3}$$

while the individual sample times are given by,

$$g(z) = (T/N)(b/a)\left[e^{az} - 1\right], \tag{3.4}$$

where b is the initial minimum sample spacing, a is the exponential growth rate of the sample time increments, and N is the total number of samples (pulses or sweeps). The parameters b, a, and N should be chosen such that the time instances of the radar echo samples must satisfy the 'maximum Coherent Processing Interval (CPI) that is allowed in the burst' denoted by T. Note that the final CPI can be different from this value, such that the last sample will be within T and the remaining portion of the signal till T will be zeros similar to the zero-padding case. Since zero padding does not change the performance, the time of the last echo sample can be chosen as the CPI for further processing. This is discussed in detail in subsection 3.3.5. Each of the parameters b, a and N has its own effect on the spectral ambiguous sidelobes and noise floor which will be explained in the subsequent subsections.

3.3.1. Ambiguous sidelobe structures

For a particular value of $N, b, a,$ and T the log-periodic sampling power spectrum for the point Doppler target is observed to be as shown in Fig.3.1, where the uniform 1 milli-second sampling Nyquist window is the region of -0.5 to 0.5 in the normalized frequency axis.

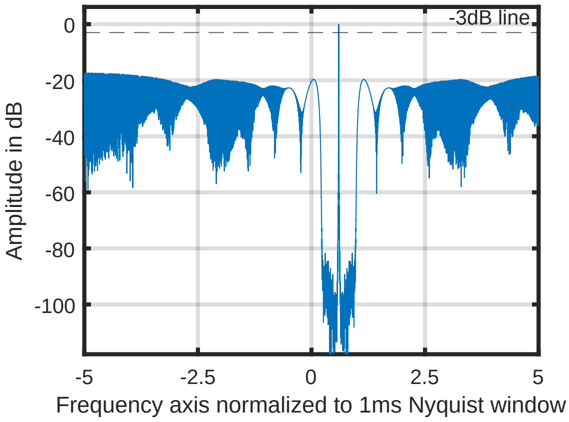

Figure 3.1: Shape of the power spectrum for log-periodic sampling with point target at 0.6 times the $1ms$ Nyquist window (which is beyond the uniform sampling unambiguous interval).

It can be observed that there are 5 distinct elements in the shape of the spectrum:

1. The **main peak** is sharp and at the exact location of the target's Doppler frequency,
2. The immediate region around the main peak has a very low noise floor and is called the **low noise floor region**,
3. Following the low noise floor region, at the location of ambiguities there are **ambiguous sidelobe structures** with a definite smooth shape,
4. The region beyond the ambiguous sidelobe structures has the **artifacts of ambiguous sidelobe suppression** which are the noise-like structures with a very high variance.
5. The spectral shape is symmetrical about the target position. Such a characteristic feature can be exploited to enhance target detection.

The specified spectral shape characteristics will be used to describe the non-uniform spectrum throughout this report. Changing the parameters in the (3.4) varies the shape of the power spectrum. The extent to which they vary and their inter-dependencies are discussed below.

3.3.2. Dependency on N

When the other parameters such as $b, a,$ and T are fixed, both the noise floor and the ambiguous sidelobe levels decrease with increasing N. This behavior is expected and is in accordance with the theory. By increasing N, we add more information about the process; which increases the quality of the power spectrum in terms of side lobe levels. Thus, when the number of samples increases, the SNR and the ambiguous sidelobe levels decrease. Thus, for best performance, the value of N should be taken to be as high as possible.

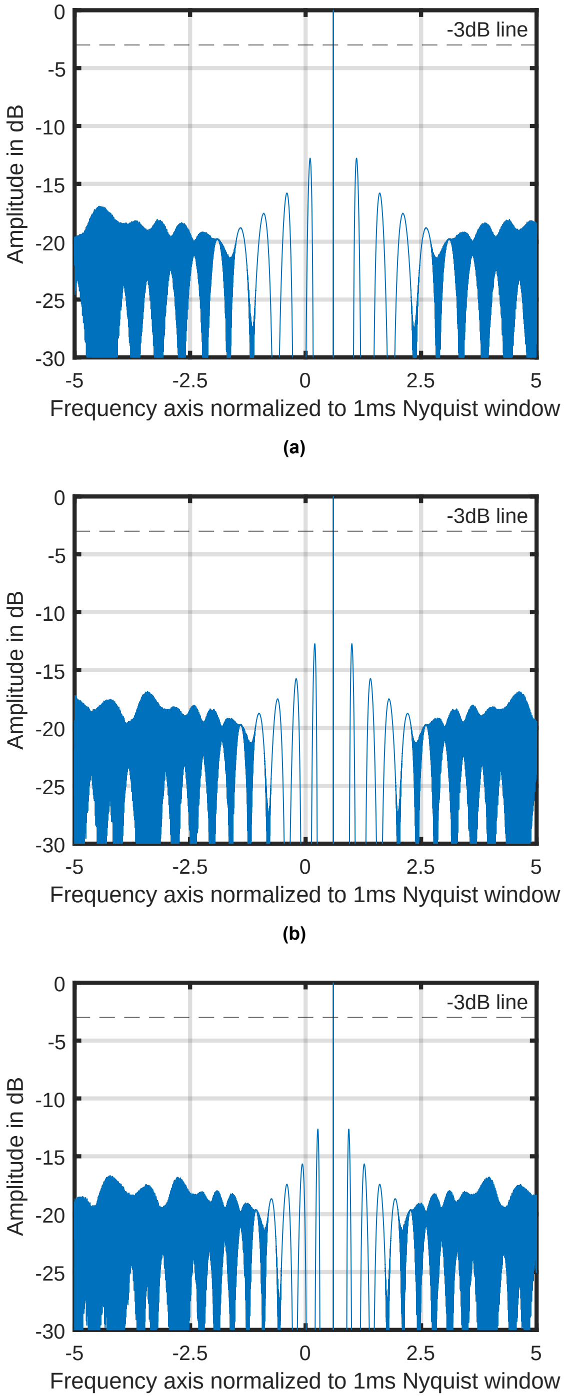

(a)

(b)

(c)

Figure 3.2: Dependency of spectral shape on b when N = 200, a = 0.002, and maximum value of T = 0.8 seconds - a) b = 0.4, ambiguous sidelobes are farther away; b) b = 0.5, ambiguous sidelobes are closer together; c) b = 0.6, ambiguous sidelobes are even more closer.

3.3.3. Dependency on b

The minimum sample spacing factor b determines the smallest time interval between the samples which is between the first and the second sample. Care must be taken to ensure that the minimum of the sample time increments denoted by (3.3), must not go below the sampling time in the uniform sampling case. The comparison taken here is for the uniform sampling case of 1 milli-second sampling, so b

b value	Minimum sample spacing due to b (in ms)	Unambiguous interval (Normalized to 1 ms Nyquist window)	Ambiguous sidelobe location (Normalized to 1 ms Nyquist window)
0.4	1.6	0.625	0.502
0.5	2	0.5	0.401
0.6	2.4	0.416666667	0.335

Table 3.1: Comparison of the different values of b and its effect on the position of ambiguous sidelobes. Here N = 200, a = 0.002, and maximum value of T = 0.8 seconds.

must be selected in such a way that for whatever combination of a, N and T, the minimum spacing is greater than or equal to 1 milli-second.

Furthermore, the effect of changing the minimum spacing influences the position of each of the successive samples. The change in the minimum sample spacing in turn changes the location of the ambiguous sidelobes. For example, when a, N, and T are fixed and selecting b such that the minimum spacing between samples is made to be 1 ms gives the ambiguous sidelobe positions to be at the same position in the case of 1 ms uniform sampling power spectrum.

Alternatively, increasing the value of b increases the minimum spacing between the samples, and the ambiguous sidelobes appear closer together. Furthermore, increasing the value of b increases the amount of artifacts due to the suppressed ambiguous sidelobes within the frequency range of interest. This effect can be observed in Fig.3.2, where the values of a, N, and T are fixed. Additionally, Table 3.1 gives the location of the ambiguous sidelobes for different values of b. It also compares the ambiguous sidelobes with the uniform sampling unambiguous interval for the same minimum spacing between samples.

3.3.4. Dependency on a

The exponential growth factor a is responsible for making the samples more non-uniform hence greatly reducing the levels of ambiguous sidelobes. Changing the value of a has four effects:

1. It changes the position of the ambiguous sidelobes and brings it closer together,
2. As a increases, the level of ambiguous sidelobes decreases,
3. As a increases, it increases the amount of artifacts due to the suppression of ambiguities,
4. As a increases, the time of the last sample (pulse or sweep) increases thereby increasing the overall CPI of the burst.

The variation of the sample spacing is shown in Fig.3.3 in which the sample spacing follows more of an exponential curved structure as the value of a increases. This curvature is directly proportional to the non-uniformity in the sample spacing and is directly proportional to reducing the ambiguities.

The power spectrum for the configuration mentioned in Figure 3.3b and Figure 3.3c is shown in Fig.3.4. The change in the position of the ambiguous sidelobes and the reason behind it is not explored as it goes too much out of the scope of this thesis. Increasing 'a' reduces the overall ambiguous sidelobe levels but also increases the amount of high-variance artifacts as observed in Figure 3.4b, which may have a larger amplitude than the smooth ambiguous sidelobes. Thus, It is more desirable to have an optimum value of a regardless of the position of the ambiguous sidelobes to achieve the best target detection performance.

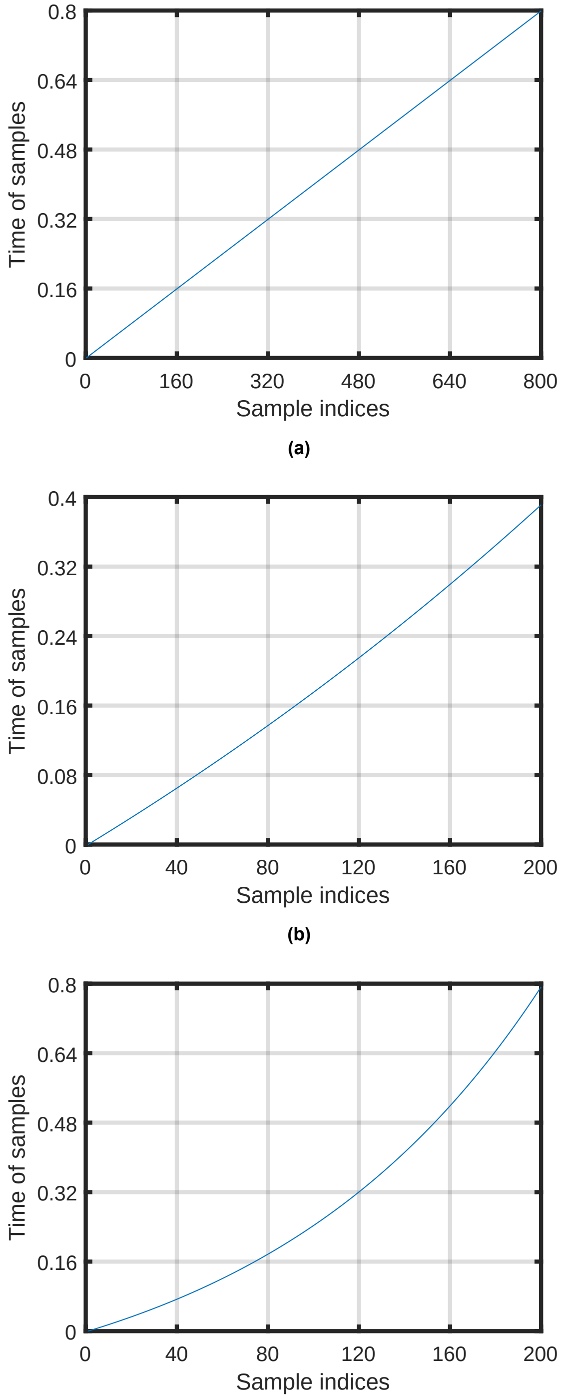

(a)

(b)

(c)

Figure 3.3: Sample timing in seconds vs Sample index for different values of a- a) uniform sampling case where each sample is spaced at 1 ms, straight line equivalent to a = 0; b) N = 200, b = 0.4, and a = 0.002 where the spacings appear slightly curved; c) N = 200, b = 0.4, and a = 0.0081 where the spacings appear significantly more curved

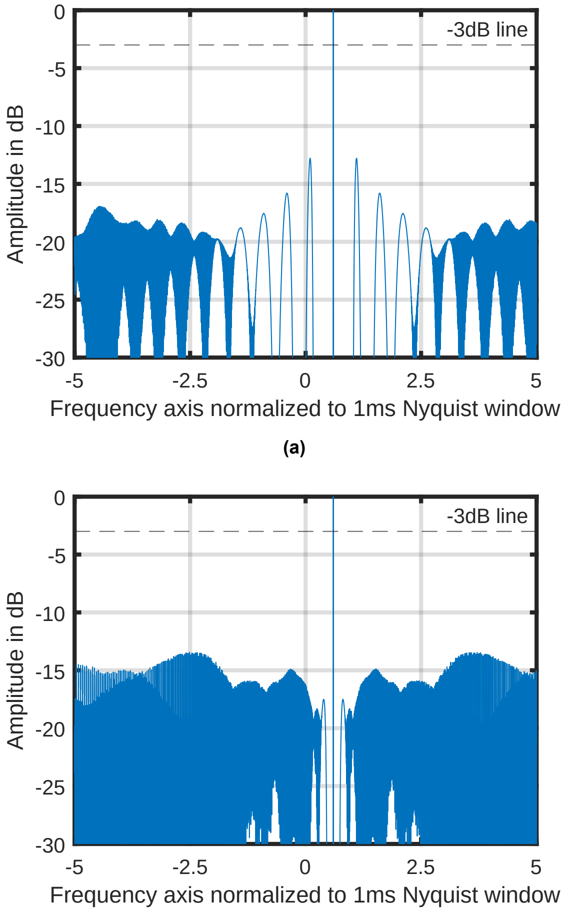

(a)

(b)

Figure 3.4: Power spectrum for different values of a for N = 200, b = 0.4 - a) a = 0.002, here the ambiguous sidelobes are large ; b) a = 0.0081, the ambiguous sidelobes are smaller but at different positions

3.3.5. Dependency on CPI

The effect of the power spectrum with respect to the overall CPI is interdependent on the values of the other parameters. It is possible to increase the CPI just by increasing the value of $N, b,$ or a individually. Alternatively, an increase in CPI can also be achieved by changing more than one of the parameters, and in such a scenario the overall effect is a complex superposition of the individual effects combined. It is also possible to get better performance by selecting an optimum set of parameters (N, b, a), rather than trying to maximize each parameter individually. This is because the parameters are interdependent on each other and the combined effect can be exploited. For example, consider Figure 3.2b where the ambiguous sidelobes are above the -15 dB level with CPI = 0.489 seconds and Figure 3.4b where the artifacts due to ambiguous sidelobe suppression are above -15 dB level with CPI = 0.792 seconds, but if the two configuration are appropriately combined then the resulting burst configuration gives better results as shown in Fig.3.5 where the CPI = 0.681 seconds. Here it can be observed that the overall ambiguous sidelobe and the artifacts due to sidelobe suppression do not exceed the -15 dB level. Thus CPI is a derived parameter separate from T, and CPI as a standalone parameter does not determine the detection performance.

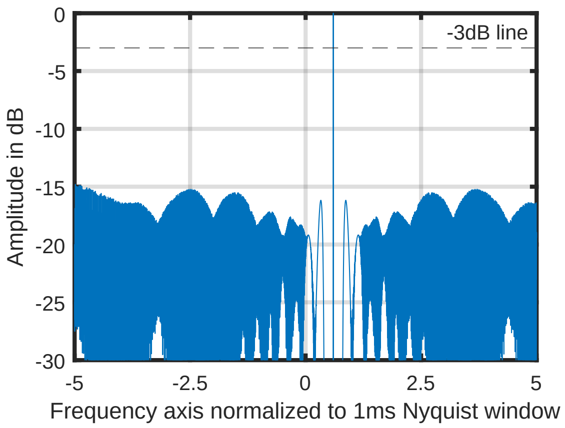

Figure 3.5: Power spectrum for N = 200, b = 0.5, a = 0.005 and maximum value of T = 0.8 seconds

3.4. Optimization of the configuration

As mentioned in the previous section, each of the parameters has a certain effect on the overall power spectrum of the signal. In order to get the highest noise floor with low ambiguous sidelobes, it is required to make some optimization of the parameters. Since (3.4) denotes the time instance and the power spectrum is obtained by doing the Fourier transform at these time instances, it is not possible to linearize and find the optimum convex solution easily. Nevertheless, by analyzing the effects each parameter has on the power spectrum the following conclusions can be made:

1. The time index of the last sample (final CPI) must not exceed the specified T (maximum burst CPI),
2. Increasing N,b or a individually increases the CPI,
3. N will always be smaller than the uniform sampling case to maintain the minimum spacing of 1 milli-second,
4. N and b are directly proportional to each other in order to maintain the minimum spacing,
5. N and b are inversely proportional to a to maintain the same CPI,
6. Increasing a increases the non-uniformity of the samples and makes the ambiguous sidelobe levels lower.
7. By having the actual CPI close to T, the best utilization of the entire signal is possible leading to the best performance.

By using the above conclusions, limits for parameter optimization can be derived. The behavior of the artifacts due to ambiguous sidelobe suppression is too erratic to analyze and so the biggest challenge in optimization is to ensure a minimum SNR after encompassing all these effects.

Generally, as the maximum possible CPI (T) increases the amount of non-uniform samples (N) in the optimized set of parameters also increases, this contributes to the better SNR as discussed in subsection 3.3.2. The values of the parameters taken for the plots (T = 0.8 seconds for 1 ms minimum sample spacing) are quite high and cannot be expected in a real-time scenario. Although the sampling structure and sample count can be preserved if the minimum sample spacing is 0.1 ms then T can be made as small as 80 ms to yield the same performance. But for a fast-scanning radar, the time on target is limited and hence the maximum CPI possible T is also limited which hinders the performance if the PRT/SRT is high. An alternative approach to mitigate this limitation is discussed below in chapter 4.

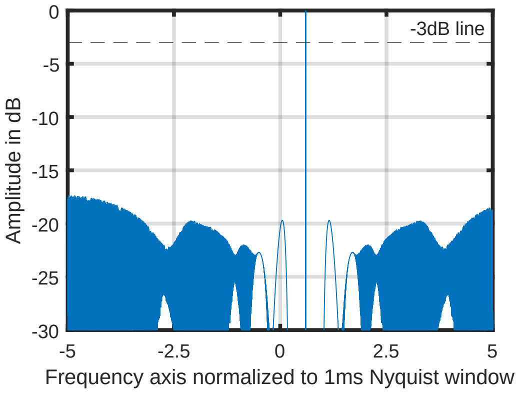

Figure 3.6: Point target at 0.6 times the normalized 1 milli-second Nyquist frequency for log-periodic sampling with N = 638, b = 0.85813899, a = 0.000472337 with T = 0.8 s.

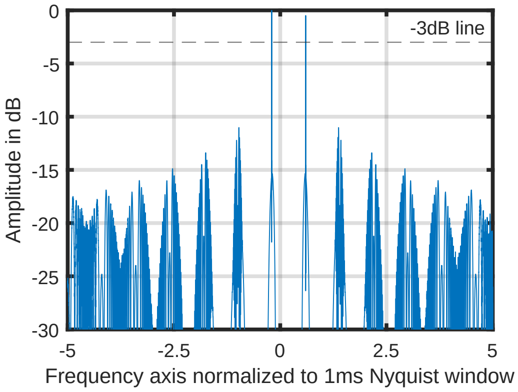

Figure 3.7: Point target at 0.6 times the normalized 1 milli-second Nyquist frequency for log-periodic sampling with N = 638, b = 0.85813899, a = 0.000472337 with T = 0.8 s.

Initially, the optimization is done with only the effect of these parameters. Later, it was found that the optimization needs to incorporate the spectrum shape of the extended targets. This can be done by ensuring that the ambiguous sidelobes are as far away as possible from the required Doppler frequency interval of estimation. Unfortunately, this was not pursued due to the lack of time and only the sub-optimal configuration is used in this thesis.

3.5. Point target performance

Using the optimization guidelines from section 3.4 and a simple $'fmincon'$ optimizer, the following values were obtained for the different parameters N = 638, b = 0.85813899, a = 0.000472337 with T = 0.8 seconds resulting in a final CPI of 0.79972 seconds. This set of parameters yields very good results overall as shown in Fig.3.6 as opposed to Fig.3.5. If the region of interest is 2 or 3 times the 1 ms Nyquist window of the uniform sampling case with 1 ms spacing, then it can be observed that the ambiguous sidelobes are of the same level but the artifacts of the sidelobe suppression are reduced to around -25 dB.

Furthermore, in the case of multiple targets, the resultant spectrum of the log-periodic sampling is the superposition of the individual target spectra. This is verified by Fig.3.7 where there are two point targets at the locations of ambiguous sidelobes of other target's spectrum. The overall spectrum looks shows the superposition along with the interferences between the individual target spectra.

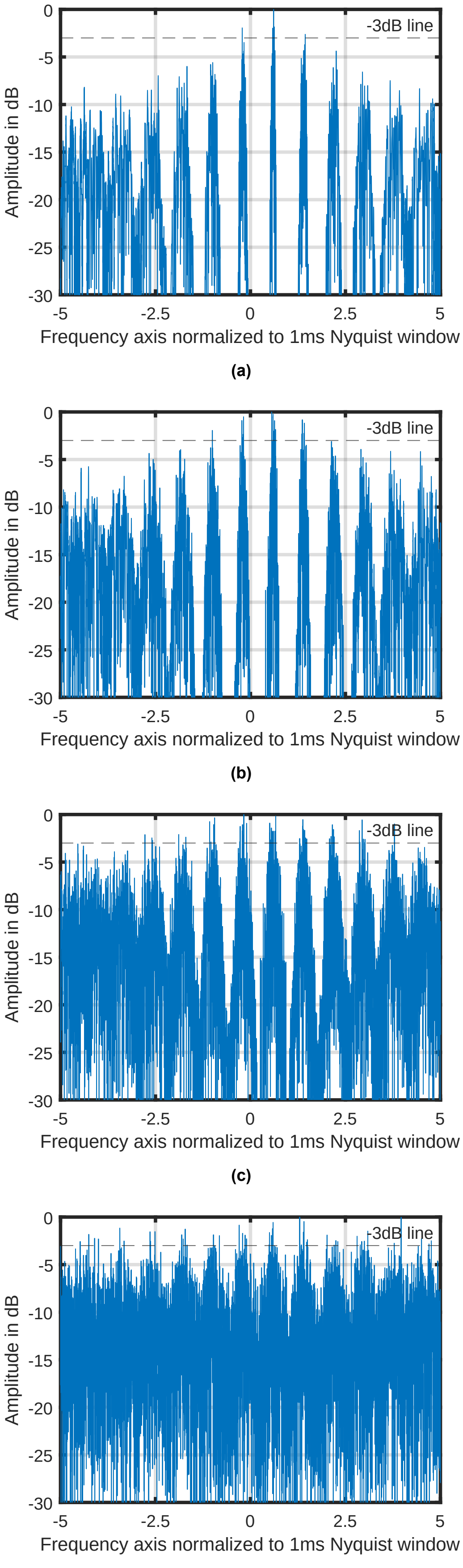

(a)

(b)

(c)

(d)

Figure 3.8: Extended target at 0.6 times the normalized 1 milli-second Nyquist frequency for log-periodic sampling with N = 638, b = 0.85813899, a = 0.000472337 with T = 0.8 seconds with different target standard deviation normalized to 1 milli-second Nyquist window a) Target standard deviation of 0.025 times ; b) Target standard deviation of 0.05 times ; c) Target standard deviation of 0.1 times ; d) Target standard deviation of 0.2 times

3.6. Extended target performance

Since the meteorological targets are loosely bound structures, different parts of these targets move with different velocities, and hence their overall Doppler velocity is a distribution over an inherent mean velocity as in the case of clouds moving with the wind. This causes such targets to have an extended Doppler spectrum. The performance of the log-periodic sampling for targets with different Doppler widths is discussed here.

For the extended target scenario, the power spectrum of log-periodic sampling for 1000 targets with standard deviations of $\frac{1}{40}^{th}$, $\frac{1}{20}^{th}$, $\frac{1}{10}^{th}$, and $\frac{1}{5}^{th}$ times the 1 milli-second Nyqust window is shown in Fig.3.8. Here there is no noise added to the signal and even so, for extended targets with multiple scatterers, the ambiguous sidelobe levels are quite high and the target is still found to be ambiguous.

Although optimization has increased the performance in the case of point targets, for the extended target scenario the performance is still inadequate. Additionally, It can be evidently observed that as the target standard deviation increases, the ambiguous sidelobe levels also increase. For the point target case shown in Fig.3.6, the main lobe is more narrow than the ambiguous sidelobes. Considering the extended target response to be the summation of the responses of many point targets, as the target standard deviation increases the narrow main lobe responses are more scattered around the mean than falling on a single frequency. But the ambiguous sidelobes are wider since there is some overlap and constructive interference of the ambiguous sidelobes of the individual responses. Hence the ambiguous sidelobes are higher for higher target standard deviation.

3.7. Conclusion

In this chapter, the analytical modeling of the extended target Doppler frequency and the log-periodic sampling technique is discussed. This is followed by an in-depth investigation of the power spectrum and its structure for the log-periodic sampling case. Each of the parameters of log-periodic sample time spacing N, b, a and T have their own effect on the power spectra. Their individual effects and the reasoning behind them are studied in detail. Furthermore, the inter-dependencies and tradeoffs between the parameters are also explored. Finally, the outline for optimization of the parameters to get the best SNR response is shown along with the performance of the optimized values. If T is fixed to be high, then the optimized values give a good resulting spectrum with lower sidelobes. But for fast scanning radars where the maximum time on target is limited, the optimized values do not perform well. For the case of point Doppler targets, the resulting spectrum from optimized values gives superior performance when compared to all the other de-aliasing techniques with an SNR level of around 17 dB for 10 times the 1 ms Nyquist window. But for the case of extended targets even without noise, the performance is still poor with high ambiguous sidelobe levels and it is found that the performance degrades with an increase in target standard deviation.

Chapter References

[7] A. W. Doerry. *Radar Doppler processing with nonuniform PRF*. Tech. rep. 2017. DOI: `10.2172/1373645`.

[8] L. Eyer and P. Bartholdi. “Variable stars: Which Nyquist frequency?” In: *Astronomy and Astrophysics Supplement Series* 135.1 (Feb. 1999), pp. 1–3. DOI: `10.1051/AAS:1999102`.

[9] J. T. VanderPlas. “Understanding the Lomb–Scargle Periodogram”. In: *The Astrophysical Journal Supplement Series* 236.1 (May 2018), p. 16. DOI: `10.3847/1538-4365/aab766`.

[13] F. Particke et al. “Additive random sampling for radar signal processing”. In: *2017 IEEE-APS Topical Conference on Antennas and Propagation in Wireless Communications, APWC 2017* 2017-January (Oct. 2017), pp. 93–96. DOI: `10.1109/APWC.2017.8062250`.

[14] M. W. Maciejewski et al. “Nonuniform sampling and spectral aliasing”. In: *Journal of Magnetic Resonance* 199.1 (July 2009), pp. 88–93. DOI: `10.1016/J.JMR.2009.04.006`.

[15] D. S. Zrnić. “Simulation of Weatherlike Doppler Spectra and Signals”. In: *Journal of Applied Meteorology and Climatology* 14.4 (June 1975), pp. 619–620. DOI: `10.1175/1520-0450(1975)014`.

[16] R. J. Doviak, D. S. Zrnic, and D. S. Sirmans. “Doppler Weather Radar”. In: *Proceedings of the IEEE* 67.11 (1979), pp. 1522–1553. DOI: `10.1109/PROC.1979.11511`.

4

Periodic non-uniform log-periodic sampling

4.1. Periodic Non-Uniform (PNU) sampling

Periodic Non-Uniform (PNU) sampling is the sampling of a signal at intervals that are not equally spaced and repeated over a period [17], [18]. PNU sampling also known as multicoset sampling is better suited for non-packable signals (signals with frequency components at the edge or beyond the Nyquist limit). This sampling method is also effective in retaining the information of the original signal [19]. PNU sampling is comparable to multi-burst processing in radar systems, where each burst has a set of non-uniform samples. The sampling scheme within each burst can be chosen from any non-uniform sampling scheme (random sampling, gaussian sampling, sinusoidal sampling, etc). Since log-periodic sampling is found to yield better performance than most of the other non-uniform sampling schemes [7]. Each of the bursts is sampled with log-periodic sampling as stated in chapter 3. The performance of PNU log-periodic sampling is evaluated for the optimized values subject to each of the burst duration as the maximum CPI (T) time period.

In the case of a Fast-scanning weather radar, the time on target is limited, and hence T is small. In such cases, it is possible to use the reflected echos from multiple scans (multiple rotations in case of a fast-rotating radar) together in the form of PNU sampling. Regardless of the bursts being incoherent (measured at instances separated by the scan time), the spectral performance is better than the case of a single burst scenario. The performance of the multi-burst PNU sampling for the case of point targets and extended targets is discussed below.

4.2. Point target performance

The performance of point target Doppler velocity spectrum estimation with PNU is evaluated as a function of the number of bursts. The first case is for the bursts that are immediately following each other with the minimum spacing time (1 milli-second) between them. The second case is for the bursts that are incoherent i.e, separated by an integer multiple of the burst duration.

4.2.1. Continuous Bursts - Point targets

For the optimized values discussed in section 3.5, the continuous bursts have a CPI almost equal to T with 0.8 seconds where the spacing between the bursts is 0.1 milli-seconds to ensure that the same uniform sampling scenario can be used for comparison. The spacing for a 5-burst scenario is shown in Fig.4.1. It can be observed that the log-periodic sampling curve for the chosen configuration is repeated 5 times. A Hanning window is then added over the entire set of multi-burst samples before applying the DFT. The entire signal after windowing is shown in Fig.4.2.

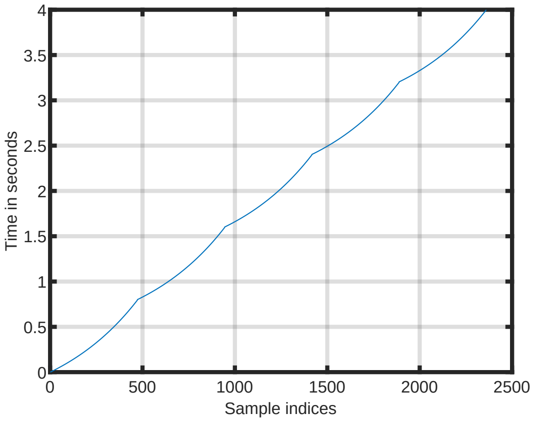

Figure 4.1: Sample spacing in seconds vs sample index for PNU sampling with log-periodic spacing within a burst with the values of N = 638, b = 0.85813899, a = 0.000472337 with T = 0.8 seconds.

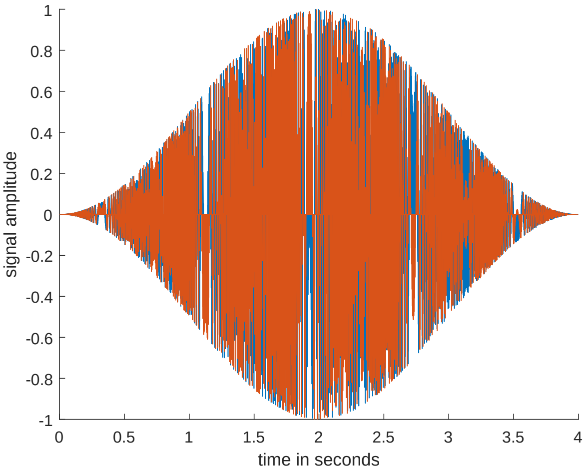

Figure 4.2: Raw signal for the case of 5-burst PNU sampling with log-periodic spacing within a burst with Hanning window applied.

In order to test the performance of multi-burst PNU, we consider three cases, the 2-burst case, the 3-burst case, and the 6-burst case of log-periodically spaced radar echoes. The power spectrum for point targets for the mentioned cases of PNU log-periodic sampling is shown in Fig.4.3. This spectrum is obtained for the optimized configuration (i.e. N = 638, b = 0.85813899, a = 0.000472337 with T = 0.8 seconds) as discussed in section 3.4. For the case of a single burst, the ambiguous sidelobes and the artifacts due to sidelobe suppression are distinguishable.

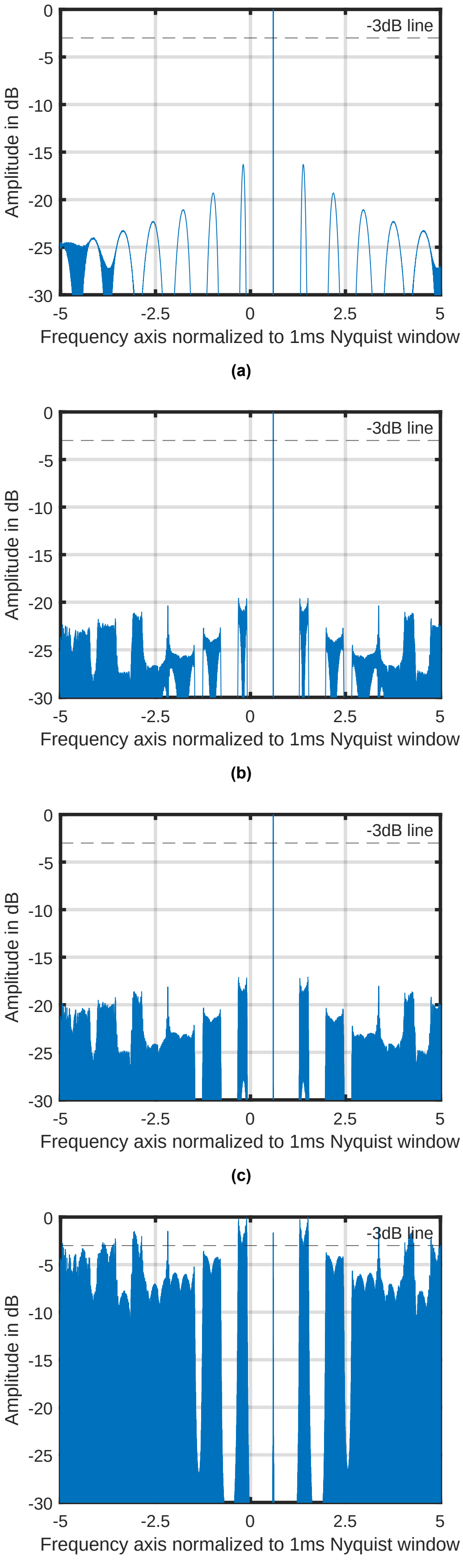

(a)

(b)

(c)

(d)

Figure 4.3: Spectrum of Point target at 0.6 times the normalized 1 milli-second Nyquist frequency for PNU log-periodic sampling with N = 638, b = 0.85813899, a = 0.000472337 with T = 0.8 seconds. a) 1 Burst case equivalent to simple log-periodic sampling without any PNU sampling (same as Fig.3.6); b) 2 Burst case c) 3 Burst case ; d) 6 Burst case

As the number of bursts increases for the point target case, two significant changes occur:

1. The ambiguous sidelobes (which have a smooth and wider spectrum at the ambiguity locations) are replaced by the high-variance artifacts,
2. The artifacts due to ambiguous sidelobe suppression (which have a high variance) increase in amplitude,

The first effect is favorable since the noise-like structure can be suppressed by the IAA algorithm, discussed in chapter 5, while the second effect of the increase in the amplitude of the high variance artifacts is undesirable. The overall effect of increasing bursts can be thought of as a tradeoff between the well-defined ambiguous sidelobes and the amplitude of the high-variance artifacts created due to suppression.

For the 2-burst case, it is observed that there is interference of ambiguous sidelobes, this results in the lowering of sidelobe level as shown in Figure 4.3b. Additionally, the power spectral density shows how the smooth ambiguous sidelobes are replaced by the higher variance artifacts. But as the number of bursts used for processing increases, the high variance artifacts at the ambiguity positions also increase. When processing signals with a continuous burst count of 6 or higher, the power level of the artifacts goes beyond the target power level, which makes this configuration infeasible for higher burst counts.

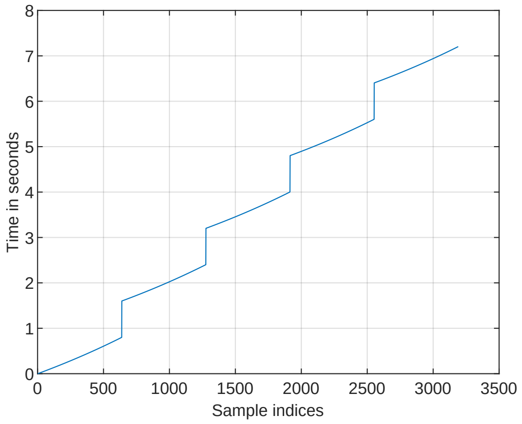

Figure 4.4: Sample spacing in seconds vs sample index for non-coherent PNU sampling with log-periodic spacing within a burst with the values of N = 638, b = 0.85813899, a = 0.000472337 with T = 0.8 seconds.

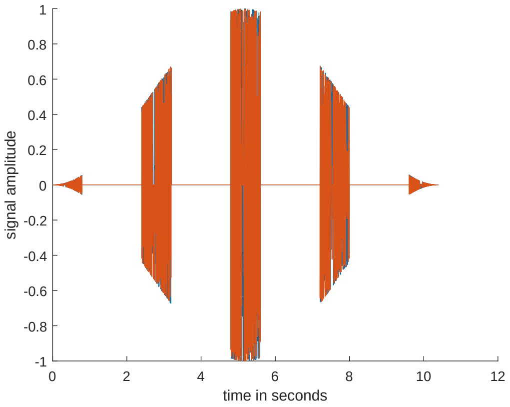

Figure 4.5: Raw signal for the case of non-coherent 5-burst PNU sampling with log-periodic spacing within a burst with the values of N = 638, b = 0.85813899, a = 0.000472337 with T = 0.8 seconds.

4.2.2. Non-Coherent Bursts (PNU-NCB) - Point targets

The PNU non-coherent burst (PNU-NCB) is another type of PNU sampling where the bursts have a time gap between them. For a fast-scanning radar, the time on target is limited and the scan time is small. Thus, the time between consecutive bursts in the same voxel is small. One aspect which can be exploited is that for multiple bursts meteorological targets can be expected to be stationary. Therefore, multiple bursts can be used to analyze the target without the effects of target migration. Since the bursts are separated in time, coherence between the samples cannot be expected.

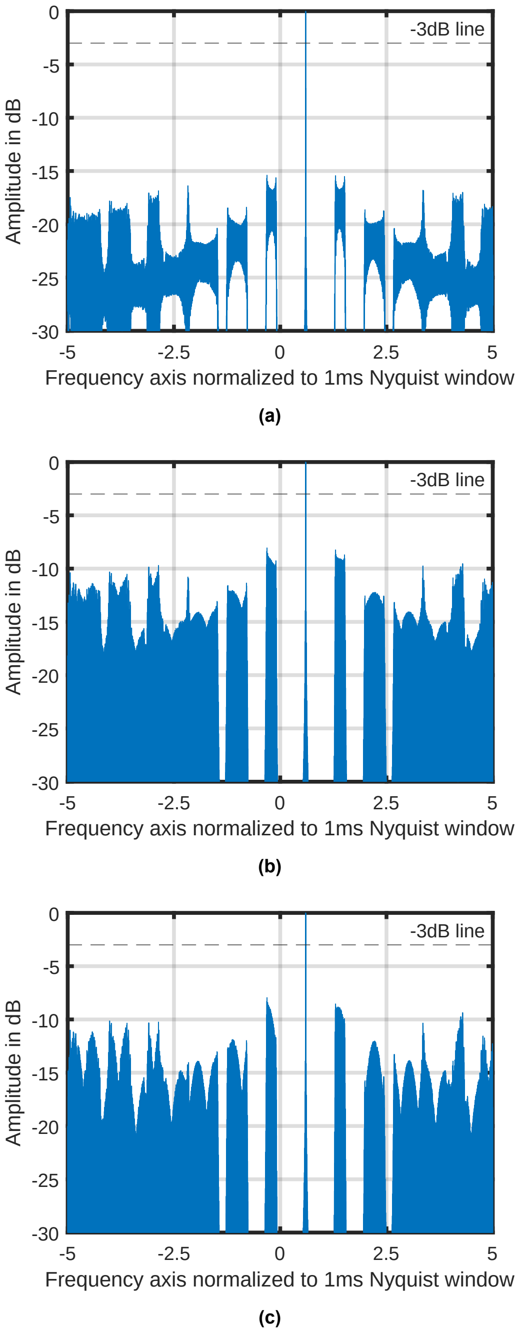

Figure 4.6: Spectrum of Point target at 0.6 times the normalized 1 milli-second Nyquist frequency for non-coherent PNU log-periodic sampling with N = 638, b = 0.85813899, a = 0.000472337 with T = 0.8 seconds and spacing between the samples as 1.601 seconds (approximately equivalent to 2 burst duration). a) 3 Burst case ; b) 6 Burst case ; c) 10 Burst case

It is proven that even by using such non-coherent samples in PNU multi-burst case, it is possible to get better performance. The spacing for a non-coherent 5-burst scenario is shown in Fig.4.4. Here, the time jump between the successive bursts is equal to one burst duration. The raw signal with the gaps between bursts is shown in Fig.4.5, where the Hanning window is applied to the entire sample set used for processing.

The power spectrum for the PNU-NCB with log-periodical samples inside the burst is shown in Fig.4.6. For the one burst case, the power spectrum is the same as the one in Figure 4.3a. With multiple trials, it is found that better performance can be obtained when the time between bursts is made to be 1 milli-second higher than two burst durations (1.601 seconds, where each burst duration is approximately 0.8 seconds).

Comparing the 6-burst cases of Figure 4.3d and Figure 4.6b, the ambiguous sidelobe levels do not increase beyond a particular level for the case of PNU-NCB as the number of bursts is increased. Unlike the continuous burst case, the ambiguous sidelobe levels do not exceed the target power level for PNU-NCB. As shown in Figure 4.6c the sidelobe levels remain constant even when 10 bursts are used for PNU-NCB but in Figure 4.3d even for 6 bursts the target amplitude is lower than the ambiguities. Hence, by using PNU-NCB, it is possible to use as many bursts as possible without having the sidelobe level above -7.5 dB.

Finally, as the number of bursts increases the smooth structured ambiguous sidelobes get suppressed more, and only the high-variance artifacts remain. By varying the burst count (from 1 burst to 10 burst for PNU-NCB) or the inter-burst spacing (1 burst-spacing to 6 burst-spacing) it is observed that the sidelobe levels do not change by more than 3dB. With multiple trials, it is found that using 6 bursts yields good results with clearly distinguishable targets. For point targets, the ambiguous sidelobes in PNU-NCB maintain a lower level even as the burst count increases. This phenomenon is advantageous for the fast-scanning radar scenario, hence PNU-NCB is suggested to be used.

4.3. Extended target performance

The Extended target performance for the case of different numbers of bursts in the case of continuous bursts (honoring the 1 milli-second minimum sample spacing between bursts) and for incoherent bursts (where the bursts are separated in time making the samples uncorrelated) are shown.

4.3.1. Continuous Bursts - Extended targets

The waveform configuration with continuous bursts for the case of the extended targets is the same as discussed in subsection 4.2.1. The extended target is made of 1000 equal scatterers having a mean Doppler frequency of 0.6 times the normalized 1 milli-second Nyquist frequency (which is already beyond the 1 milli-second Nyquist window of -0.5 to 0.5 Normalized frequency) with a Gaussian target standard deviation of 0.025, 0.05, 0.1 and 0.2 times the normalized 1 milli-second Nyquist frequency.

Although using 6 bursts in PNU resulted in very high sidelobe levels for the point Doppler target scenario, for extended Doppler targets using 6 bursts yields good performance. The power spectrum for 6-burst PNU with log-periodic sampling is shown in Fig.4.7. In comparison with Fig.3.8, it can be clearly observed that the ambiguous sidelobes are reduced significantly when 6 bursts are used instead of 1. Unfortunately, the performance becomes worse (increase in the amplitude of the High-variance artifacts) as the target standard deviation increases.

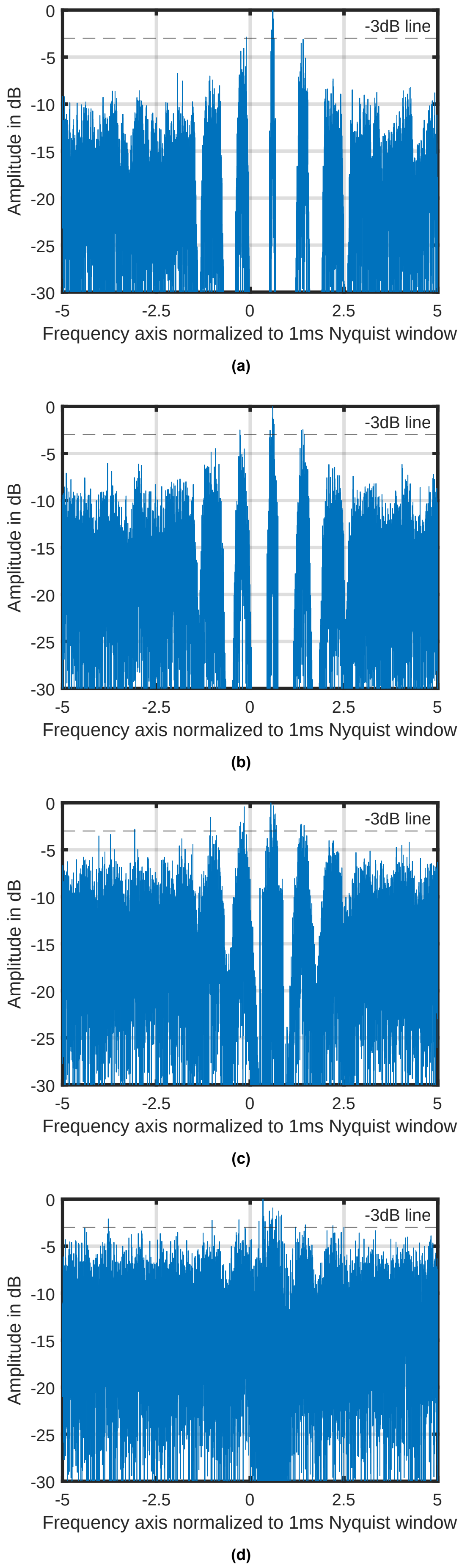

(a)

(b)

(c)

(d)

Figure 4.7: Spectrum of extended targets for different standard deviation located at 0.6 times the normalized 1 milli-second Nyquist window for PNU log-periodic sampling continuous bursts with N = 638, b = 0.85813899, a = 0.000472337 with T = 0.8 seconds for 6 burst case with frequency normalized to 1-milli-second Nyquist window. a) Target standard deviation = 0.025 times ; b) Target standard deviation = 0.05 times ; c) Target standard deviation = 0.1 times ; d) Target standard deviation = 0.2 times

Additionally, increasing the number of bursts enables better distinguishable targets from the artifacts created due to suppression as can be observed in Figure 4.7c and Figure 4.7d when compared with Fig.3.8. Thus, if a sufficient number of bursts are used for processing then target detection becomes easier, but estimating the target's moments is still error-prone due to the presence of ambiguous sidelobe structure and high-variance artifacts.

4.3.2. Non-Coherent Bursts - Extended targets

From the discussion in subsection 4.2.2, for higher burst count PNU-NCB is effective in removing ambiguities without any increase in the ambiguous sidelobe level for the point target case. Here, the same waveform is applied for extended targets with different target Doppler standard deviations. The power spectrum for the PNU-NCB 6 bursts with the spacing of 1.601 seconds between the bursts is shown in the Fig.4.8.

Here for targets with lower standard deviation ($\leq$ 0.025 times the 1 milli-second Nyquist window), the level of the artifacts due to ambiguity suppression is lower than that continuous burst case. When comparing Fig.4.7 and Fig.4.8, the performance is slightly better for PCU-NCB than continuous bursts. Additionally, PCU-NCB is more suitable for Fast-scanning radars since the bursts are separated in time.

Although PCU-NCB performs well regardless of most spacings between the bursts, care must be taken so that the burst spacing does not induce additional periodicity in the signal which can cause unnecessary complications.

4.4. Conclusion

Periodic Non-uniform (PNU) sampling is done by using repetitions of a particular sampling strategy as multi-burst processing to enhance the performance. Log-periodic sampling when compared with PNU with the overall same duration (regardless of the inter-burst spacing) has better performance. But since the time on target for the fast-scanning radar is limited, Periodic Non-Uniform (PNU) sampling can be used. It enables the use of multiple short non-uniformly sampled bursts to enhance target spectral detection capabilities. The maximum burst count is limited by the time taken for target migration. The optimized log-periodic parameters are used for spacing inside the burst. The use of PNU along with log-periodic sampling is a novel contribution done in this thesis. Furthermore, enabling this waveform to be used in fast-scanning radars but setting the inter-burst spacings is also a novelty proposed which has been verified to give good results.

Increasing the number of bursts replaces the smooth ambiguous sidelobes around the target with the high-variance artifacts of ambiguous sidelobe suppression. In the continuous burst case, the bursts are immediately following each other and the increase in burst count increases the ambiguous sidelobe levels for the case of point targets.

Alternatively, when the bursts are separated in time there is a minor increase in performance. This suits the operations of a Fast-scanning radar since the scan-to-scan time can be incorporated as the spacing between bursts. This gives rise to a variation of the waveform as Periodic Non-Uniform Non-Coherent Bursts (PNU-NCB). The PNU-NCB for the 6-burst case with inter-burst spacing equal to 2 times the burst duration (1.601 milli-seconds) is found to be better in performance and its performance is shown.

In contrast to the continuous burst case, increasing the number of non-coherent bursts (irrespective of the inter-burst spacing) does not increase the ambiguous sidelobe levels for point Doppler targets. Thus it is advantageous to use PNU-NCB rather than PNU continuous bursts for processing.

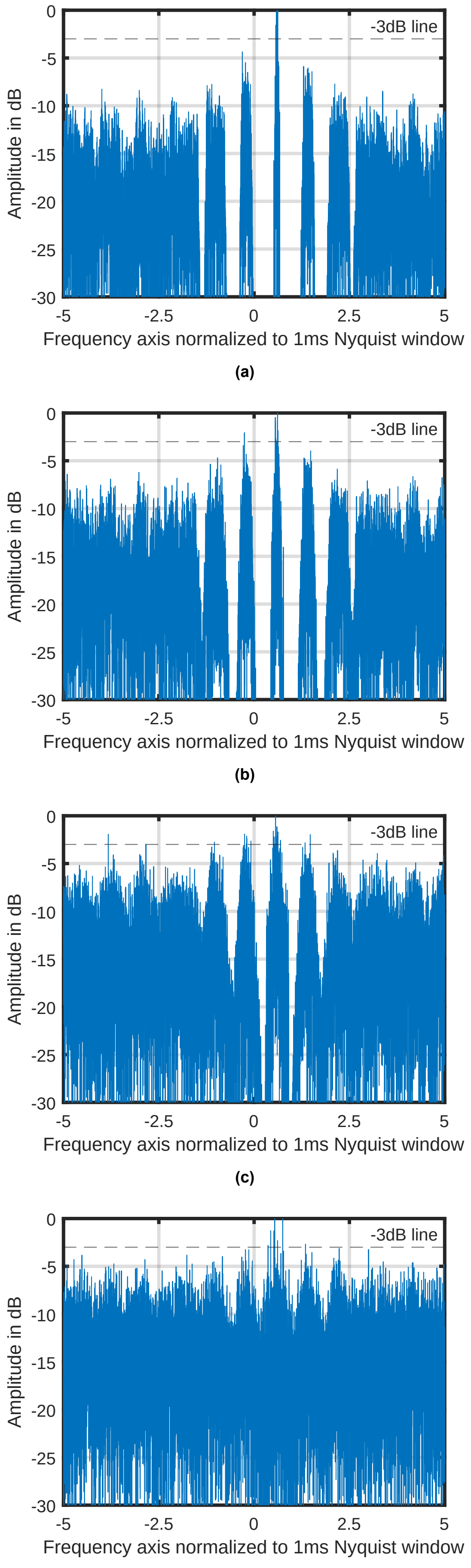

(a)

(b)

(c)

(d)

Figure 4.8: Spectrum of extended targets for different standard deviation located at 0.6 times the normalized 1 milli-second Nyquist window for PNU-NCB with N = 638, b = 0.85813899, a = 0.000472337 with T = 0.8 seconds for 6 burst case with frequency normalized to 1-milli-second Nyquist window. a) Target standard deviation = 0.025 times ; b) Target standard deviation = 0.05 times ; c) Target standard deviation = 0.1 times ; d) Target standard deviation = 0.2 times

Chapter References

[7] A. W. Doerry. *Radar Doppler processing with nonuniform PRF*. Tech. rep. 2017. DOI: `10.2172/1373645`.

[17] R. H. Kestur. “Application of periodic nonuniform sampling for detection of radar signals”. In: (2017).

[18] S. Zhao et al. “Modifications on Multichannel Reconstruction Algorithm for SAR Processing Based on Periodic Nonuniform Sampling Theory and Nonuniform Fast Fourier Transform”. In: *IEEE Journal of Selected Topics in Applied Earth Observations and Remote Sensing* 8.11 (Nov. 2015), pp. 4998–5006. DOI: `10.1109/JSTARS.2015.2421303`.

[19] M. Rashidi. “Non-uniform sampling and reconstruction of multi-band signals and its application in wideband spectrum sensing of cognitive radio”. In: *ArXiv* (2010).

5

IAA algorithm

5.1. IAA Introduction

Iterative Adaptive Approach (IAA) Algorithm is a non-parametric and hyperparameter-free, weighted least-squares-based iterative adaptive approach to suppress the noise in the signal [20] [6]. IAA was initially used for amplitude and phase estimation in the array processing domain. The non-parametric nature enables the algorithm to be used for any target shape and the hyperparameter-free approach ensures that no tuning is required. IAA can work well with one or a few snapshots that are uncorrelated, partially correlated, and/or coherent sources with arbitrary sample spacings. Each burst in the multi-burst PNU log-periodic sampling can be translated into one signal snapshot for the IAA algorithm. Unlike conventional algorithms, IAA does not rely on multiple signal snapshots to estimate the covariance matrix. Some of the other algorithms used for target detection are the Clairvoyant estimator, Standard Capon beamformer (SCB), and MUltiple SIgnal Classification (MUSIC) [21]. IAA is a parameter-free data-adaptive spectrum estimator which can perform better than the algorithms mentioned above [20] and has the following salient features:

1. Provides robust estimation with a single data snapshot;
2. Applicable to non-uniform sampling grid;
3. Maintain high spectral resolution to resolve ambiguities;
4. Do not require setting parameters, which affect the estimation;
5. Robust against the possible presence of correlated noise (clutter).

IAA was originally proposed for source localization in antenna array beamforming [20], but has been used to remove the sidelobes in many applications [22] [23] [6]. In this thesis, the IAA algorithm has been translated from source localization to spectral estimation using sample times. The inherent similarity between both the domain is evident and the signal processing is analogous.

5.2. IAA Original Data model

In this section, the original data model pertaining to source localization is shown and the translation of it for the radar scenario is also discussed. IAA tries to estimate the noise-free version of the signal using a Weighted Least Squares cost function at every location or frequency bin i as given by,

$$f_{1,i} = \left(\mathbf{y} - x_i \mathbf{a}\left(\theta_i\right)\right)^H \mathbf{K}^{-1}\left(\theta_i\right)\left(\mathbf{y} - x_i \mathbf{a}\left(\theta_i\right)\right) \tag{5.1}$$

Here, **y** is the received signal and **x** is the noise-free signal to be retrieved. The vector $\mathbf{a}(\boldsymbol{\theta})$ is the steering vector in the case of source localization and it encompasses the Fourier basis for the Doppler frequency estimation. The covariance matrix $\mathbf{K}^{-1}(\theta_i)$ defines the interference coming from all other locations, considering that other targets are present in the scene. For the Doppler estimation scenario, it defines the interference, noise, and ambiguous sidelobes. The structure of the covariance matrix [6] is:

$$\mathbf{K}(\theta_i) = \sum_{j=1,j\neq i}^{N_t N_v} |x_j|^2 \mathbf{a}(\theta_j)\mathbf{a}^H(\theta_j) = \mathbf{R} - |x_i|^2 \mathbf{a}(\theta_i)\mathbf{a}^H(\theta_i), \tag{5.2}$$

where N_t and N_v are the number of grid points in the range and velocity accordingly which satisfies $N_t N_v > LM$. Here L is the count of adjacent range cells that are large enough to encompass the response of the target during the whole CPI and M is the number of pulses/sweeps in the CPI. The matrix **R** is given by

$$\mathbf{R} = \sum_{j=1}^{N_t N_v} |x_j|^2 \mathbf{a}(\theta_j)\mathbf{a}^H(\theta_j) \tag{5.3}$$

Maximizing Weighted Least Squares criteria (5.1) with respect to x_i gives:

$$x_i^{\text{IAA}} = \frac{\mathbf{a}^H(\theta_i)\mathbf{K}^{-1}(\theta_i)\mathbf{y}}{\mathbf{a}(\theta_i)^H\mathbf{K}^{-1}(\theta_i)\mathbf{a}(\theta_i)}. \tag{5.4}$$

Applying matrix inverse lemma to (5.4) gives:

$$x_i^{\text{IAA}} = \frac{\mathbf{a}^H(\theta_i)\mathbf{R}^{-1}\mathbf{y}}{\mathbf{a}(\theta_i)^H\mathbf{R}^{-1}\mathbf{a}(\theta_i)}. \tag{5.5}$$

Solving (5.5) and (5.3) in an iterative manner gives an estimation of $\hat{\mathbf{x}}^{\text{IAA}} = \left[x_1^{\text{IAA}}, \ldots, x_{N_t N_v - 1}^{\text{IAA}}\right]^T$. The initialization for IAA is done by normal Discrete Fourier Transform (DFT). The clutter covariance matrix model (5.3) implies that the number of point-like targets in the scene can be as many as $KM-1$, leaving one degree of freedom to the noise.

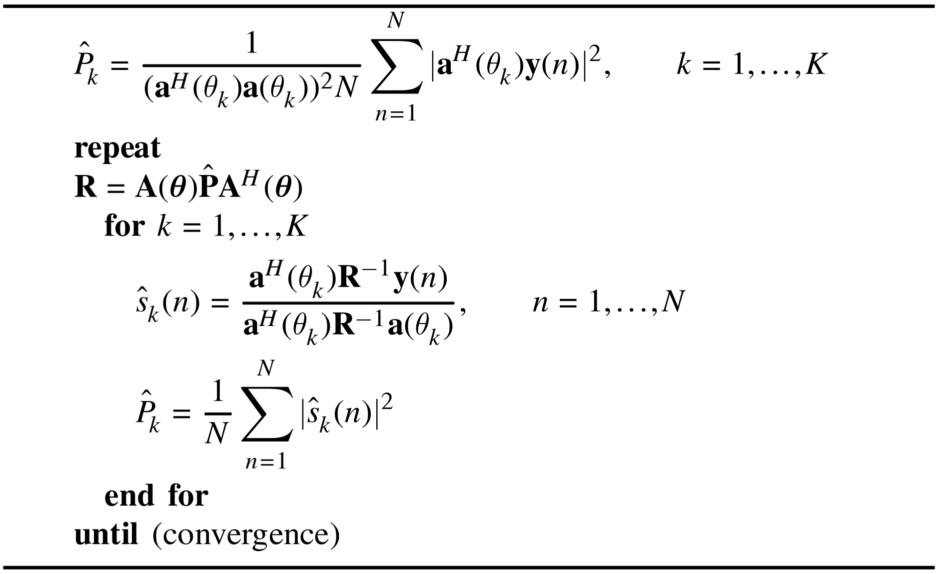

```
$\hat{P}_k = \frac{1}{(\mathbf{a}^H(\theta_k)\mathbf{a}(\theta_k))^2 N} \sum_{n=1}^{N} |\mathbf{a}^H(\theta_k)\mathbf{y}(n)|^2, \quad k = 1,\ldots,K$
repeat
$\mathbf{R} = \mathbf{A}(\boldsymbol{\theta})\hat{\mathbf{P}}\mathbf{A}^H(\boldsymbol{\theta})$
  for $k = 1,\ldots,K$
    $\hat{s}_k(n) = \frac{\mathbf{a}^H(\theta_k)\mathbf{R}^{-1}\mathbf{y}(n)}{\mathbf{a}^H(\theta_k)\mathbf{R}^{-1}\mathbf{a}(\theta_k)}, \quad n = 1,\ldots,N$
    $\hat{P}_k = \frac{1}{N} \sum_{n=1}^{N} |\hat{s}_k(n)|^2$
  end for
until (convergence)
```

Figure 5.1: IAA algorithm structure

The IAA implementation structure is given in Fig.5.1, where $n = 1, ..., N$ denotes the number of snapshots, $k = 1, ..., K$ denotes the frequency bin index and $\hat{\boldsymbol{P}}$ denotes the K x K diagonal matrix containing the spectral amplitude of each bin $\hat{P}_k$ as the diagonal elements.

5.3. Performance

Until now, all the simulations in the previous chapters were done by using ideal signals without noise. In order to find the effectiveness of IAA, the simulations are repeated with complex noise determined from a user-defined SNR of 30 dB added to the signals as mentioned in [15].The performance of the IAA algorithm for different target types and different types of waveforms is shown below. The waveform configuration is kept the same with the optimized log-periodic configuration of N = 638, b = 0.85813899, a = 0.000472337 with T = 0.8 seconds for a single burst. For the PNU-NCB case, 6 bursts with an inter-burst spacing equal to 2 times the burst duration are used.

The number of iterations is usually set from 5 to 15 for the estimation to reach convergence [6]. The convergence criteria are the mean Doppler, Doppler standard deviation, and averaged noise floor, if the change in these values is minimal then the spectrum is assumed to be converged. For the considered extended targets, it is found that convergence is attained at different iterations depending on target Doppler widths and the level of noise in the received signal. In multiple trials, it is found that for 30 dB SNR, the convergence takes at max 10 iterations. Care must be taken to ensure that for low-noise cases, the matrix $\boldsymbol{R}^{-1}$ is close to a singular matrix and may yield incorrect values.

5.3.1. Log periodic sampling - Point targets

For the single burst with log-periodic sample spacing, IAA performance is tested with an additive noise level of 30 dB SNR. In this subsection, we only look at the performance for the case of point targets. The time taken for the IAA algorithm is mainly due to the inversion of $\boldsymbol{R}$ matrix which is an NxN matrix, thus as the number of pulses/sweeps within a burst increases the computational time also increases.

The power spectrum for different IAA iterations is shown in Fig.5.2. IAA suppresses the ambiguous sidelobes to have an SNR of 30 dB after 1 IAA iteration. The power spectrum converges with just 2 iterations for the point target case with the converged spectrum having a minimum SNR of 40 dB.

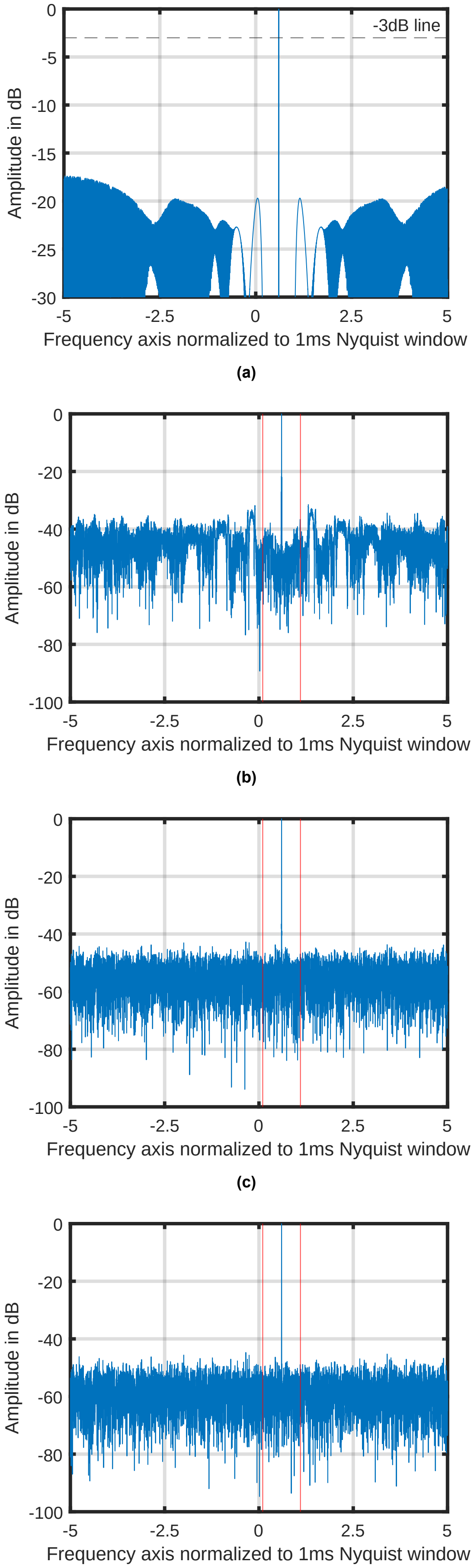

(a)

(b)

(c)

(d)

Figure 5.2: Spectrum of point target at 0.6 times the normalized 1 milli-second Nyquist window for log-periodic sampling for the 6-burst case for different IAA iterations. a) Power spectrum before applying IAA (same as Fig.3.6) ; b) Power spectrum after 1 IAA iteration ; c) Power spectrum after 2 IAA iteration ; d) Power spectrum after 4 IAA iteration ;

5.3.2. Log periodic sampling - Extended targets

The IAA algorithm has superior performance for the point Doppler target case since the noise-free power spectrum matrix $\hat{\boldsymbol{P}}$ has a clear diagonal structure. For the extended target case, the performance of the algorithm at 10 iterations is shown in Fig.5.3.

Compared with Fig.3.8, the extended target spectrum after 10 IAA iterations show the targets clearly, and the ambiguous sidelobes are suppressed. Although, for the wider Doppler targets, the ambiguous sidelobe levels are still quite high.

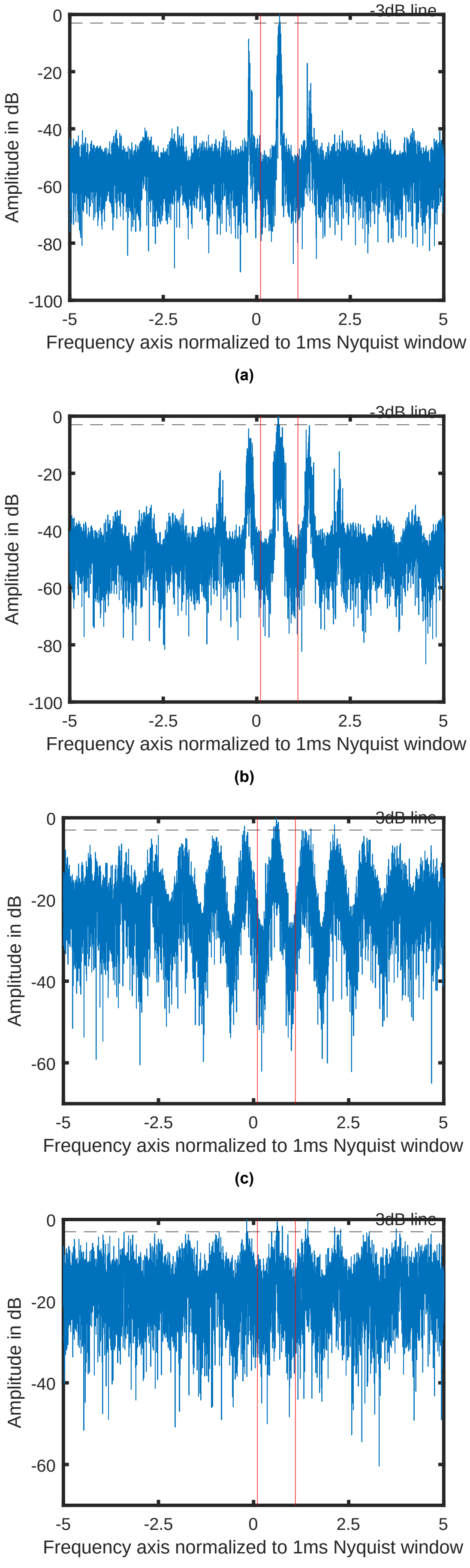

Figure 5.3: Spectrum of extended targets with Doppler mean 0.6 times the normalized 1 ms Nyquist window with log-periodic sampling for the 6-burst case for different target Doppler widths. a) 0.025 times the $1ms$ Nyquist window ; b) 0.05 times the $1ms$ Nyquist window ; c) 0.1 times the $1ms$ Nyquist window ; d) 0.2 times the $1ms$ Nyquist window ;

5.3.3. PNU with log-periodic bursts - Point targets

For the case of PNU-NCB with 6 bursts and inter-burst spacing of 2 bursts time, the IAA performance for point targets is shown for different iterations.

Here the spectrum converges at the 4^{th} iteration as shown in Figure 5.4d with the converged spectrum having a minimum SNR level of 50 dB, which is better than the single burst case by approximately 10 dB when compared with Figure 5.2d.

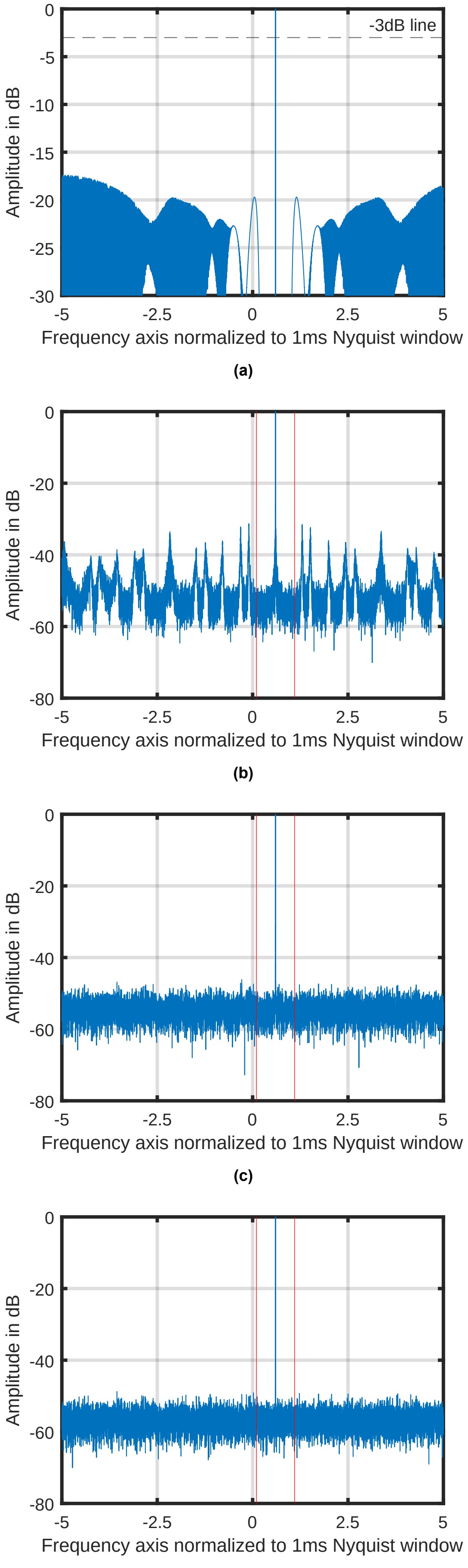

(a)

(b)

(c)

(d)

Figure 5.4: Spectrum of point target at 0.6 times the normalized 1 milli-second Nyquist window for PNU-NCB sampling for the 6-burst case for different IAA iterations. a) Power spectrum before applying IAA (same as Fig.3.6) ; b) Power spectrum after 1 IAA iteration ; c) Power spectrum after 2 IAA iteration ; d) Power spectrum after 4 IAA iteration ;

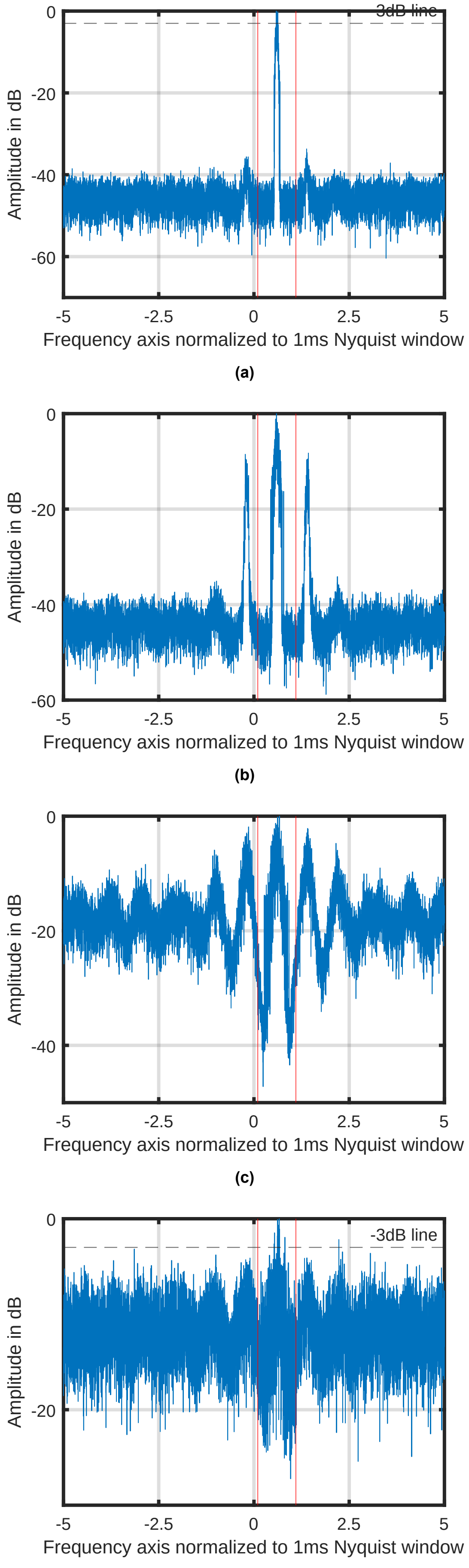

(a)

(b)

(c)

(d)

Figure 5.5: Spectrum of extended targets at 0.6 times the normalized 1 milli-second Nyquist window for PNU-NCB for the 6-burst case after 10 IAA iterations. a) Target standard deviation of 0.025 times ; b) Target standard deviation of 0.05 times ; c) Target standard deviation of 0.1 times ; d) Target standard deviation of 0.2 times ;

5.3.4. PNU with log-periodic bursts - Extended targets

Now, the same waveform configuration is applied for different target Doppler widths, and the power spectrum after 10 IAA iterations is shown in Fig.5.5.

For target detection, the maximum of the estimated power spectrum is taken as the center of the 1 milli-second minimum spacing Nyquist window. Then, the Doppler mean and the standard deviation estimation is done over this 1 milli-second Nyquist window.

Additionally, IAA has the effect of suppressing the lowest points in the target power spectral width as shown in Fig.5.6. Here the red circled point inside the target spectrum is suppressed by the algorithm. This is because IAA assumes a diagonal covariance matrix structure as it tries to minimize the effect of interference. Although this effect occurs, the inherent shape of the target is preserved even for multiple iterations and so IAA does not affect the estimation of the first and the second Doppler moments (mean and standard deviation) of the target.

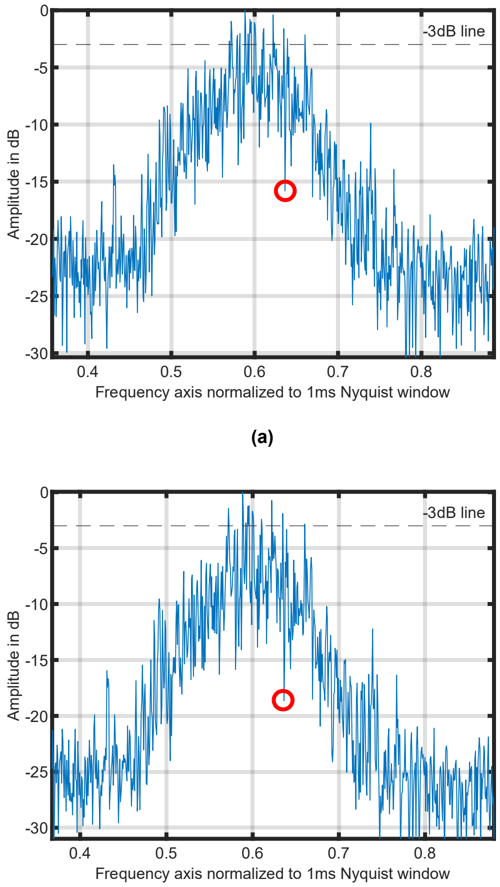

(a)

(b)

Figure 5.6: Zoomed target spectrum of an extended target at 0.6 times the normalized 1 milli-second Nyquist window with 0.05 times the Nyquist window as the target standard deviation. a) Power spectrum after 1 IAA iteration ; b) Power spectrum after 10 IAA iteration ;

5.4. Drawbacks

The convergence and the statistical properties of IAA are still the subject of ongoing research. So far, only local convergence of IAA has been proved [22]. That is done by demonstrating that IAA is an approximated Maximum Likelihood Estimator (MLE) in a multi-target scenario.

Since IAA is an iterative approach the time for convergence is higher as it depends on the number of iterations required. The time taken per iteration is primarily due to the computation of the inverse matrix $\boldsymbol{R}^{-1}$ which is a NxN matrix where N is the total number of samples (pulses/sweeps) within a burst. The computation time also depends on the number of signal snapshots that are used for the covariance matrix estimation. For the PNU-NCB with 6-burst case, it takes around 45 seconds for each matrix inversion using MATLAB when run on a 4-core CPU.

The number of iterations required for convergence varies with the noise level in the signal and the target Doppler standard deviation. This makes the overall computation time vary over a wide range.

Additionally, because IAA assumes that the covariance matrix is a diagonal matrix, it may lead to a larger than necessary reduction of the number of degrees of freedom when some of the interfering sources are coherent. This is because the cancellation of multiple coherent interfering sources would require only one degree of freedom if the correct structure of the covariance matrix were known [20]. However, the true structure of the covariance matrix is assumed to be unknown for this thesis.

5.5. Conclusion

The performance of IAA for the optimized configuration is tested for the single burst case and for PNU-NCB with 6 bursts. The number of iterations required for convergence is depended on the following factors:

1. It is inversely proportional to the number of bursts or snapshots being used,
2. It is inversely proportional to the noise level in the signal (for higher noise levels, the computation time is lower and the final SNR after convergence is also lower),
3. It is dependent on the target Doppler standard deviation.

For signals with an input of 30 dB SNR, the maximum number of iterations required for convergence is 10 regardless of target Doppler standard deviation.

The overall computational time is the product of the number of iterations and the time taken for each iteration. The time taken for each iteration is directly proportional to the number of samples per burst and the total number of snapshots of the signal used. With multiple trials, it is found that the computation time is lower for signals with higher noise levels. For such cases, the converged spectral SNR decreases with higher input noise, this behavior is expected.

Chapter References

[6] N. Petrov. “Migrating Target Detection in Wideband Radars”. In: *TU Delft Repositories* (). DOI: `10.4233/uuid:08556a7c-ef90-43f7-998b-f103ceea6267`.

[15] D. S. Zrnić. “Simulation of Weatherlike Doppler Spectra and Signals”. In: *Journal of Applied Meteorology and Climatology* 14.4 (June 1975), pp. 619–620. DOI: `10.1175/1520-0450(1975)014`.

[20] T. Yardibi et al. “Source localization and sensing: a nonparametric iterative adaptive approach based on weighted least squares”. In: *IEEE Transactions on Aerospace and Electronic Systems* 46.1 (Jan. 2010), pp. 425–443. DOI: `10.1109/TAES.2010.5417172`.

[21] N. Petrov and F. Le Chevalier. “Iterative adaptive approach for unambiguous wideband radar target detection”. In: *2015 European Radar Conference, EuRAD 2015 - Proceedings* (Dec. 2015), pp. 45–48. DOI: `10.1109/EURAD.2015.7346233`.

[22] W. Roberts et al. “Iterative adaptive approaches to MIMO radar imaging”. In: *IEEE Journal on Selected Topics in Signal Processing* 4.1 (Feb. 2010), pp. 5–20. DOI: `10.1109/JSTSP.2009.2038964`.

[23] P. Stoica, P. Babu, and J. Li. “New method of sparse parameter estimation in separable models and its use for spectral analysis of irregularly sampled data”. In: *IEEE Transactions on Signal Processing* 59.1 (2011), pp. 35–47. DOI: `10.1109/TSP.2010.2086452`.

6

Results and discussions

6.1. Introduction

This chapter focuses on the simulated theoretical performance of the PNU-NCB waveform structure along with the IAA algorithm as discussed in the previous chapter of this report. Additionally, experimental verification of the performance of the log-periodic sampling along with the signal processing steps used is discussed. The ultimate goal of the thesis is to unambiguously estimate the target mean and standard deviation for extended targets. Although the synthesized waveform and IAA algorithm perform well, validation of the target's unambiguous estimation performance is needed. A Monte Carlo simulation is done for multiple input SNR values, burst count, IAA iterations, and target Doppler width. This showcases the performance over multiple trials when a random noise signal is generated for each trial.

Experimental verification is also done by using the PARSAX radar [24] of TU Delft. PARSAX is short for 'Polarimetric Agile Radar in S and X band' which is a highly configurable polarimetric FMCW radar [25]. The targets are taken as the vehicles on the roads and highways around TU Delft. The results are in line with the performance of non-uniform sampling.

6.1.1. Doppler Moments Estimation

The Doppler moments which help in characterizing a target, can be found by using the equations following equations [26]. The total power or zeroth moment of Doppler (P_T) is given by

$$P_T = \int_{-f_{amb}}^{+f_{amb}} |S(f)|^2 df \tag{6.1}$$

where $S(f)$ is the estimated Doppler spectrum found by applying the DFT as mentioned in section 2.4, $-f_{amb}$ and $+f_{amb}$ denote the 1 milli-second Nyquist window, df is the Doppler frequency resolution.

The mean Doppler frequency μ can be calculated using,

$$\mu = \frac{1}{P_T} \int_{-f_{amb}}^{+f_{amb}} f|S(f)|^2 df$$

Consecutively, the Doppler spectrum width can be found by using the following relation,

$$\sigma = \sqrt{\int_{-f_{amb}}^{+f_{amb}} \frac{1}{P_T}[f-\mu]^2 |S(f)|^2 df}$$

All of the mentioned moments estimation equations are inherently defined for the case of uniform sampling and hence are calculated using the entire Nyquist window for which there are no ambiguities. In order to use these equations for the non-uniform sampling case, the Nyquist window must be fixed over the extended frequency range before estimation. This is done by finding the maximum of the spectrum and using that point as the center for the 1 milli-second Nyquist window. The Doppler moments are then estimated inside this window.

6.2. Monte-Carlo Simulations

A Monte-Carlo simulation is done for 100 trials for the PNU-NCB waveform. For each trial, a signal is generated with a specified input SNR level and target spectral width. Then, the estimation is done after applying IAA. The configuration of the Monte-Carlo simulation is as follows:

- Input SNR = 10 dB, 20 dB and 30 dB;
- Target spectral width = 0.01, 0.025, 0.05, 0.1, and 0.2 times the 1 milli-second Nyquist window;
- Number of burst in PNU-NCB = 1, 3,and 6;
- maximum IAA iterations = 10.

Here when the number of bursts in PNU-NCB is one, it emulates the simpler log-periodic sampling case. Since the convergence criteria had been validated to be achieved at 10 bursts, the Monte-Carlo simulation is made to have the maximum IAA iteration count as 10. The results of the simulation are shown below.

6.2.1. Target Dopper mean estimation

As discussed in subsection 5.3.4, it can be concluded that the possibility of false peaks is prominent in the case of wider targets (0.1 and 0.2 times the Nyquist window). These false peaks affect the position of the 1 milli-second Nyquist window placement and consequently the mean estimation. Thus, the results of the Monte-Carlo simulations are shown only for these two cases of target spectral width.

Since the ambiguous sidelobes are high and the Doppler spectrum has a low SNR for extended Doppler targets, we define a range for the correct mean estimation with respect to the target standard deviation. If the estimated mean is found to be within the range of (-0.5σ,0.5σ) and (-0.75σ,0.75σ) from the actual mean for target spectral widths (normalized to $1ms$ Nyquist window) of 0.1 and 0.2 respectively, then the estimate is assumed to be correct.

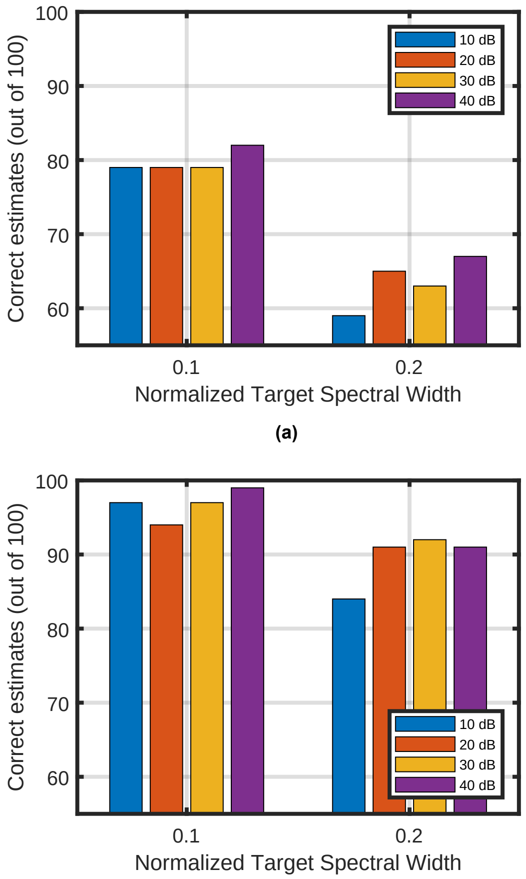

(a)

(b)

Figure 6.1: Bar Graph showing the number of correct target mean estimations (out of 100) after 10 IAA iterations for different input SNR values and for 2 target Doppler widths. a) 3 burst case ; b) 6 burst case ;

From Fig.6.1, the distribution of the correct estimates for both the spectral widths and the different input SNR values can be observed. As expected from the IAA performance plots in Fig.5.5, the estimation is better for the case of lower noise levels and for lower target spectral widths. Additionally, the performance enhancement associated with the increase in the number of bursts is also verified.

6.2.2. Target spectral width estimation

For the target spectral width estimation, all of the estimations for the 100 Monte-Carlo cases are centered around the same value. The estimated vs true spectral width for different input SNR values is shown in Fig.6.2.

From Fig.6.2, it can be observed that the narrower targets ($\leq$ 0.1 times the Nyquist window) are estimated more accurately in the 3-burst and 6-burst cases than in the 1-burst case. Since the typical Doppler standard deviation for meteorological targets is between $1/20$ th and $1/30$ th of the size of the Nyquist window [16], it is favorable to use multiple bursts for such cases. Additionally, to show the effect of multiple bursts the estimated vs true spectral width for the different number of bursts for the 30 dB input SNR case is shown in Fig.6.3.

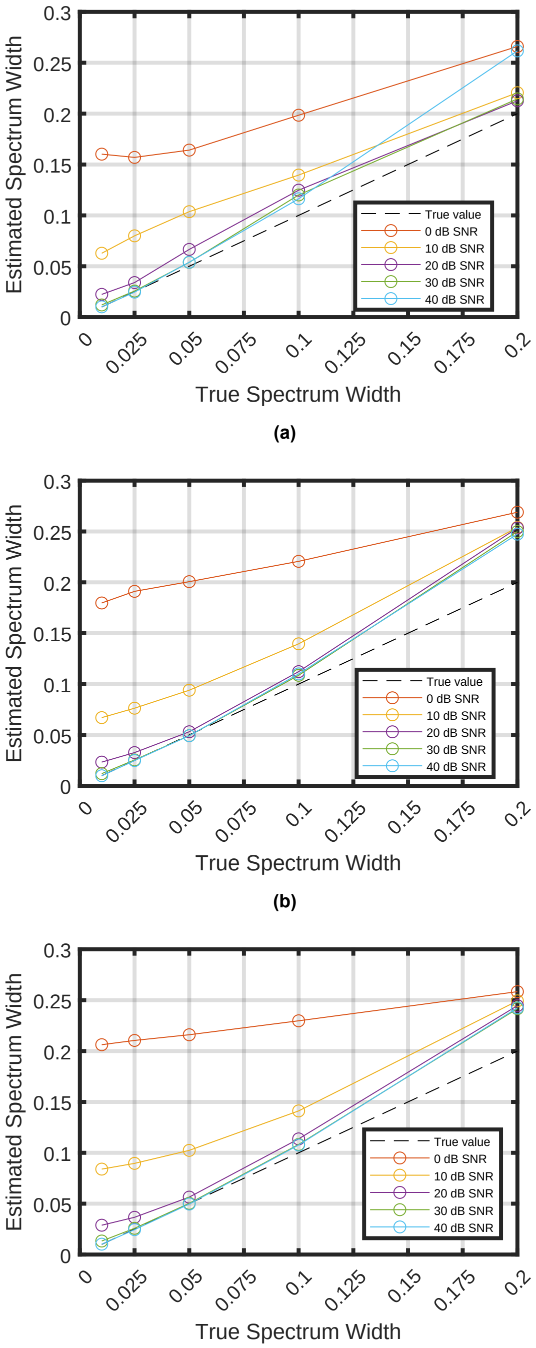

(a)

(b)

(c)

Figure 6.2: Estimated vs True spectral width (normalized to 1 milli-second Nyquist window) for different input SNR values of the optimized PNU-NCB signal after 10 IAA iterations. a) 1 burst case (similar to log-periodic sampling ; b) 3 burst case PNU-NCB ; c) 6 burst case PNU-NCB ;

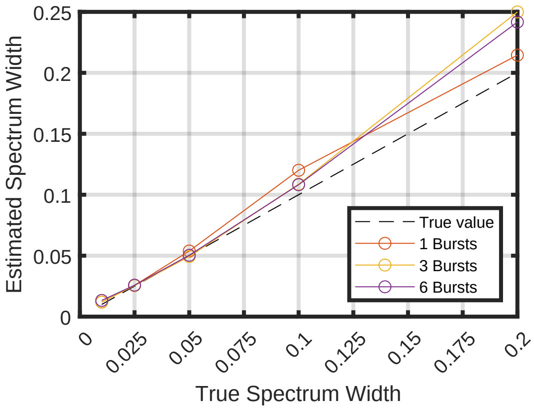

Figure 6.3: Estimated vs True spectral width (normalized to 1 milli-second Nyquist window) for different bursts for 30 dB input SNR of the optimized PNU-NCB signal after 10 IAA iterations.

From the figures, the following inferences can be concluded:

- 1-burst configuration performs well for the largest spectral width, but since the typical meteorological target spectral widths are around 0.03-0.05 times the Nyquist window. It is preferable to go for multi-burst cases to gain accuracy with targets having smaller Doppler widths
- For the targets < 0.1 times the Nyquist window, it is observed that the 3-burst case even performs slightly better than the 6-burst case. But for targets $\geq$ 0.1 times the Nyquist window, the 6-burst case performs considerably better.

Hence the 6-burst case can be taken as the optimum configuration for the estimation of the spectral width.

6.2.3. Discussion of theoretical results

The Monte-Carlo simulation results are in-line with the observations from the previous chapters. From the results and the inferences from the previous chapters, it is evident that the false peaks are due to the high levels of ambiguous sidelobes coupled with the effect of noise. This leads to incorrect spectral moments estimations. An alternative approach that can potentially reduce the number of false estimations is by exploiting the symmetrical structure of the non-uniform power spectrum to find the target position and then applying the Nyquist window to estimate the target's spectral moments.

6.3. Experimental results

The TU Delft S-band FMCW PARSAX radar [27] was used to experimentally verify the unambiguous results of log-periodic sampling observed in the simulation. For testing purposes, a Continuous Wave (CW) signal of 13 milli-seconds was transmitted and received. By using CW waveform, the processing is considerably less complex and there is no issue of range migration. The target is chosen to be moving vehicles on the highway and streets around TU Delft. Since vehicles such as cars and trucks have a fixed structure, they only have point Doppler velocities characterized by narrow peaks.

6.3.1. Experimental Setup

The radar is made to operate at S-band with a central frequency of 3.315 GHz. The performance of the log-periodic sampling was tried and verified in this radar using a CW waveform. Thus the Doppler frequency can be directly obtained by using an IQ mixer. With the $13ms$ signal, the velocity samples are assumed to be obtained for every $50\mu s$ (SRT/PRT) thus the total uniform sample count is 260 samples.

By using the optimization technique as discussed in section 3.4, the configuration obtained is N = 208, b = 0.85813899, a = 0.000472337 with T = $0.013s$ for a single burst configuration. The non-uniform samples are arranged with the spacing step accuracy of 10 ns. This enables the 50 us Nyquist window of the uniform sampling case to be extended by 5000 times by using log-periodic sampling. Comparison of the uniform sampling with the optimized configuration for log-periodic sampling along with the IAA performance is experimentally verified.

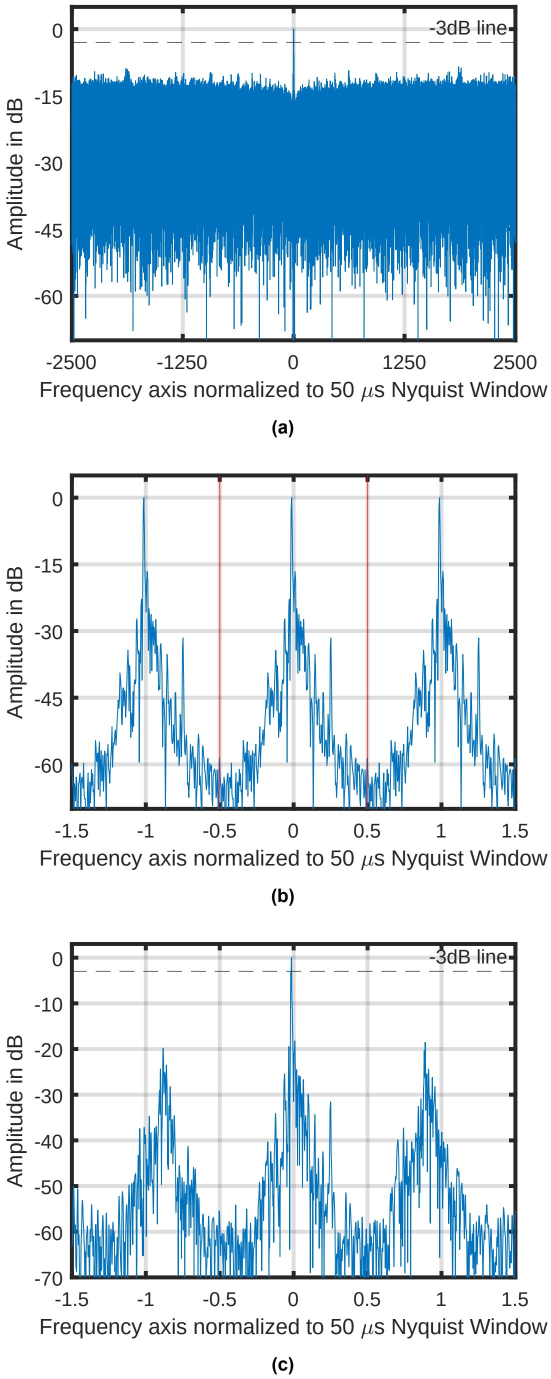

Figure 6.4: Effect of non-uniform sampling and IAA on the experimental data from PARSAX. a) Log-periodic sampling case of the extended-spectrum without ambiguities ; b) Uniform sampling case with 3 times the 50 μs Nyquist window ; c) Log-periodic sampling case with 3 times the 50 μs Nyquist window after 10 IAA iterations ;

The data received from PARSAX is noise prone and sufficient filtering needs to be done. Since we are using CW wave of 3.315 GHz, for the average car speeds the received Doppler frequency is close to the zero Doppler frequency. For example, the car traveling around 110 kmph velocity has a Doppler frequency of 400 Hz (this is very small compared to the extended unambiguous frequency range of -250 MHz to 250 MHz when 10 ns non-uniform time steps are used).

Applying the optimized log-periodic sampling strategy for the PARSAX data, the unambiguous Doppler velocity interval is enhanced by 5000 times as shown in Fig.6.4. Additionally, the IAA algorithm is found to reduce the ambiguous sidelobes from -10 dB value to around -20 dB.

6.4. Conclusion

The Monte-Carlo results show the performance of the optimized PNU-NCB burst configuration results is consistent with the inferences described in the previous chapters. The estimation of the target Doppler standard deviation is comparable to the estimation performance in the uniform sampling case [28] [26] in the presence of noise. Thus, the non-uniform sampling approach can enhance the unambiguous interval by orders of magnitude without any compromise in the target's Doppler spectral estimation.

The experimental data and results from the PARSAX radar have successfully verified the performance of log-periodic sampling and the IAA algorithm for noise suppression with real-time targets (vehicles) and noise. By considering 50 μs uniformly sampled Doppler velocity data and non-uniform sample step accuracy of 10 ns it is possible to enhance the unambiguous interval by 5000 times. Additionally, the IAA algorithm is capable of enhancing the level for ambiguous sidelobes from around -10 dB to around -20 dB for 10 iterations.

Chapter References

[16] R. J. Doviak, D. S. Zrnic, and D. S. Sirmans. “Doppler Weather Radar”. In: *Proceedings of the IEEE* 67.11 (1979), pp. 1522–1553. DOI: `10.1109/PROC.1979.11511`.

[24] O. A. Krasnov et al. “PARSAX: High-resolution Doppler-polarimetric FMCW radar with dual-orthogonal signals”. In: *18-th INTERNATIONAL CONFERENCE ON MICROWAVES, RADAR AND WIRELESS COMMUNICATIONS*. 2010, pp. 1–5.

[25] Z. Li. *Design, Simulation and Validation of Dual-channel Polarimetric Agile Radar Technology*. 2011.

[26] R. J. Doviak and D. S. Zrnić. *Doppler radar and weather observations*. Academic Press, 1993, p. 562.

[27] O. A. Krasnov et al. “The PARSAX - full polarimetric FMCW radar with dual-orthogonal signals”. In: *2008 European Radar Conference*. 2008, pp. 84–87.

[28] D. S. Zrnic. “Spectral Moment Estimates from Correlated Pulse Pairs”. In: *IEEE Transactions on Aerospace and Electronic Systems* AES-13.4 (1977), pp. 344–354. DOI: `10.1109/TAES.1977.308467`.

7

Conclusion and Recommendations

7.1. Conclusion

The unambiguous observation interval (Nyquist window) is governed by the Pulse Repetition Frequency (PRF) or Sweep repetition Frequency (SRF) of the radar, where each pulse or sweep is processed to give radar echoes in slow time. To the best of the author's knowledge, non-uniform sampling is found to be the most promising approach in literature to extend the Nyquist window.

The first of the novelties in this thesis is the adaptation of the non-uniform sampling method to Doppler frequency measurement. The non-uniform samples are structured such that the minimum spacing (PRT/SRT) does not go below the 1 ms (user-defined) uniform sampling case, to maintain a valid comparison between the results. A finer time axis is used to model the signal and then the FFT algorithm can be used to display the spectrum. The time axis is made to be finer by a factor equal to the required unambiguous interval as shown in subsection 2.4.1. Thus, in the case of 1 ms uniform samples if the non-uniform case spaces the signals with 1 μs accuracy, then a maximum improvement of 1000 times in the unambiguous Doppler interval can be observed. The extent to which the Nyquist limit is enhanced for the non-uniform sampling case has been verified and the steps on modeling the signal for a given unambiguous Doppler velocity requirement have been mentioned.

Upon comparison of the spectral estimation methods namely, modified DFT and the lomb-Scargle periodogram (a non-uniform spectral estimation algorithm), the latter is found to be more computationally intensive. Additionally, The Lomb-Scargle periodogram does not have a fixed frequency resolution, hence it is not used. The position of the non-uniform samples and the gap between them govern the signal modeling and performance. Of the several non-uniform sampling methods mentioned in the literature, log-periodic sampling is extensively explored here due to its better performance than most other methods. In log-periodic sampling, the sample times and the resulting power spectrum depend on four parameters namely - the number of samples (N), exponential growth factor (a), minimum sample spacing factor (b), and the total Coherent Processing Interval (CPI).

The relationship between these parameters on the overall spectrum has been explored. Some insights to optimize these values and optimization trials have been carried out, to yield the lowest sidelobe levels of around -19 dB for the point Doppler targets. The optimized values have been tested for different target spectral widths and the optimization performance is found to be independent of target spectral width. Although some optimization has been done, the values obtained from the optimizer converge at the local minima of the cost function. Moreover, a better cost function may be used to yield better results.

The second main novelty in this thesis work is the use of the Iterative Adaptive Approach (IAA) algorithm [20][21] to exploit the unambiguous structure of log-periodic sampling spectrum to improve the final SNR. Results show that optimized log-periodic sampling along with IAA gives very good estimation performance with less than 10% of error for targets with lower spectral width (<10% of the uniform sampling Nyquist window). But for extended targets with spectral width greater than 10% of the uniform sampling Nyquist window, the standard deviation estimation of the spectrum is overestimated by 10% to 20% of the true target standard deviation. It is found that this bias increases with the noise level in the received signal. One of the main caveats, of the IAA algorithm is the need for a matrix inversion during each iteration. The dimensions of the inversion matrix are NxN, where N is the number of Doppler samples in the non-uniform sampling case. For the 638 x 638 matrix version with 6 snapshots of the signal, it takes 45 seconds for each matrix inversion using MATLAB when run on a 4-core CPU. During multiple trials with different scenarios, it is found that 10 iterations of the IAA algorithm give the best convergence performance after which there is no significant improvement.

The third main novelty in this thesis is exploiting the fast-scanning nature of the radar to enhance spectral estimation performance. For a fast-scanning radar, it is not possible to enhance the performance of the spectral estimation by increasing the CPI. Alternatively, a stationarity assumption (meaning the frequency content in the slow-time echo sequence remains the same) helps with combining the data from several scans of the radar. By using the multi-scan data and applying it to a non-uniform sampling strategy called 'Periodic Non-Uniform Non-Coherent Burst (PNU-NCB)' sampling, it has been proven to circumvent the need for higher CPI. Here each burst has the optimized log-periodic sampling and the bursts are separated by the scan time of the radar. Even so, the impact of noise in the signal still makes the estimations unreliable. Thus an enhancement of the IAA algorithm for a multi-burst case has been developed where each burst is taken as a snapshot and the noise covariance matrix is jointly estimated. This greatly improves the performance when compared with a single burst of optimized log-periodic sampling. For point targets, we have an SNR of 50 dB with a realistic extension of the unambiguous interval by 1000 times or higher.

Monte-Carlo simulations have been performed for different Doppler spectrum widths, with different input SNR levels of random noise, and with varying numbers of bursts. The results are found to be consistent with the theory and inferences. Additionally. an experiment has been conducted with PARSAX radar using CW waveform. The received signal of 13 ms CPI with a uniform sampling time of 50 μs and is processed using the optimized log-periodic configuration with 10 ns non-uniform sample steps. It is shown that the 50 μs uniform sampling Nyquist window can be extended by 5000 times without aliasing and the SNR increases from 10 dB to 20 dB for real-time noise case after 10 IAA iterations. This proves the validity of the approach. Thus, the de-aliasing performance can be improved greatly by implementing PNU-NCB log-periodic sampling coupled with the IAA algorithm.

7.2. Recommendations for future works

Since this is the first time non-uniform sampling has been used for the estimation of Doppler target estimation, a lot has been explored with respect to the performance, dependencies, and limitations. Some of the future recommendations to further this work is mentioned below:

1. As mentioned in subsection 6.2.3, the symmetrical structure of the PNU-NCB log-periodic spectrum can be exploited to find the target position. This will in turn enhance the estimation performance as well.
2. The optimization can be made to incorporate the spectrum structure of extended targets. This can be done by ensuring that the ambiguous sidelobes are as far away as possible from the required

Doppler frequency interval of estimation. Additionally, the formulation of a convex function will enable global optimization to be possible to select the log-periodic parameters.

3. Other non-uniform sampling methods, can be used as a standalone structure or in combination with the 'periodic non-uniform' sampling approach to explore the performance. Some examples are Gaussian sampling, jittered sampling, additive random sampling, prime and co-prime number spacing sampling, Fibonacci sampling, positive and negative log-periodic sampling within the same burst, etc.
4. Lagrange Interpolation is an interpolation method using the sample points of a multi-frequency signal to reconstruct it in the time domain. A type of 'Inverse Lagrange Interpolation' can be explored along with the non-uniform sampling to reconstruct the signal spectrum without aliasing.
5. Another well-known approach in mixed-signal systems is by using 'zero crossings of entire functions' to characterize all the frequency components present in the signal. This method can also be potentially explored to provide alias-free processing.

Chapter References

[20] T. Yardibi et al. “Source localization and sensing: a nonparametric iterative adaptive approach based on weighted least squares”. In: *IEEE Transactions on Aerospace and Electronic Systems* 46.1 (Jan. 2010), pp. 425–443. DOI: `10.1109/TAES.2010.5417172`.

[21] N. Petrov and F. Le Chevalier. “Iterative adaptive approach for unambiguous wideband radar target detection”. In: *2015 European Radar Conference, EuRAD 2015 - Proceedings* (Dec. 2015), pp. 45–48. DOI: `10.1109/EURAD.2015.7346233`.

References

[1] V. Louf et al. “Unravel: A robust modular velocity dealiasing technique for doppler radar”. In: *Journal of Atmospheric and Oceanic Technology* 37.5 (May 2020), pp. 741–758. DOI: `10.1175/JTECH-D-19-0020.1`.

[2] C. N. James and R. A. Houze. “A Real-Time Four-Dimensional Doppler Dealiasing Scheme”. In: *Journal of Atmospheric and Oceanic Technology* 18.10 (2001), pp. 1674–1683. DOI: `https://doi.org/10.1175/1520-0426(2001)018<1674:ARTFDD>2.0.CO;2`.

[3] D. R. Burton et al. “Fast two-dimensional phase-unwrapping algorithm based on sorting by reliability following a noncontinuous path”. In: *Applied Optics, Vol. 41, Issue 35, pp. 7437-7444* 41.35 (Dec. 2002), pp. 7437–7444. DOI: `10.1364/AO.41.007437`.

[4] J. J. Helmus and S. M. Collis. “The Python ARM Radar Toolkit (Py-ART), a Library for Working with Weather Radar Data in the Python Programming Language”. In: *Journal of Open Research Software* 4.1 (July 2016), p. 25. DOI: `10.5334/jors.119`.

[5] J. Zhang and S. Wang. “An Automated 2D Multipass Doppler Radar Velocity Dealiasing Scheme”. In: *Journal of Atmospheric and Oceanic Technology* 23.9 (2006), pp. 1239–1248. DOI: `https://doi.org/10.1175/JTECH1910.1`.

[6] N. Petrov. “Migrating Target Detection in Wideband Radars”. In: *TU Delft Repositories* (). DOI: `10.4233/uuid:08556a7c-ef90-43f7-998b-f103ceea6267`.

[7] A. W. Doerry. *Radar Doppler processing with nonuniform PRF*. Tech. rep. 2017. DOI: `10.2172/1373645`.

[8] L. Eyer and P. Bartholdi. “Variable stars: Which Nyquist frequency?” In: *Astronomy and Astrophysics Supplement Series* 135.1 (Feb. 1999), pp. 1–3. DOI: `10.1051/AAS:1999102`.

[9] J. T. VanderPlas. “Understanding the Lomb–Scargle Periodogram”. In: *The Astrophysical Journal Supplement Series* 236.1 (May 2018), p. 16. DOI: `10.3847/1538-4365/aab766`.

[10] M. D. Migliore. “On the sampling of the electromagnetic field radiated by sparse sources”. In: *IEEE Transactions on Antennas and Propagation* 63.2 (Feb. 2015), pp. 553–564. DOI: `10.1109/TAP.2014.2379911`.

[11] N. R. Lomb. *Least-squares frequency analysis of unequally spaced data*. Tech. rep. 1976.

[12] J. D. Scargle. “Studies in astronomical time series analysis. II - Statistical aspects of spectral analysis of unevenly spaced data”. In: *The Astrophysical Journal* 263 (Dec. 1982), p. 835. DOI: `10.1086/160554`.

[13] F. Particke et al. “Additive random sampling for radar signal processing”. In: *2017 IEEE-APS Topical Conference on Antennas and Propagation in Wireless Communications, APWC 2017* 2017-January (Oct. 2017), pp. 93–96. DOI: `10.1109/APWC.2017.8062250`.

[14] M. W. Maciejewski et al. “Nonuniform sampling and spectral aliasing”. In: *Journal of Magnetic Resonance* 199.1 (July 2009), pp. 88–93. DOI: `10.1016/J.JMR.2009.04.006`.

[15] D. S. Zrnić. “Simulation of Weatherlike Doppler Spectra and Signals”. In: *Journal of Applied Meteorology and Climatology* 14.4 (June 1975), pp. 619–620. DOI: `10.1175/1520-0450(1975)014`.

[16] R. J. Doviak, D. S. Zrnic, and D. S. Sirmans. “Doppler Weather Radar”. In: *Proceedings of the IEEE* 67.11 (1979), pp. 1522–1553. DOI: `10.1109/PROC.1979.11511`.

[17] R. H. Kestur. “Application of periodic nonuniform sampling for detection of radar signals”. In: (2017).

[18] S. Zhao et al. “Modifications on Multichannel Reconstruction Algorithm for SAR Processing Based on Periodic Nonuniform Sampling Theory and Nonuniform Fast Fourier Transform”. In: *IEEE Journal of Selected Topics in Applied Earth Observations and Remote Sensing* 8.11 (Nov. 2015), pp. 4998–5006. DOI: `10.1109/JSTARS.2015.2421303`.

[19] M. Rashidi. “Non-uniform sampling and reconstruction of multi-band signals and its application in wideband spectrum sensing of cognitive radio”. In: *ArXiv* (2010).

[20] T. Yardibi et al. “Source localization and sensing: a nonparametric iterative adaptive approach based on weighted least squares”. In: *IEEE Transactions on Aerospace and Electronic Systems* 46.1 (Jan. 2010), pp. 425–443. DOI: `10.1109/TAES.2010.5417172`.

[21] N. Petrov and F. Le Chevalier. “Iterative adaptive approach for unambiguous wideband radar target detection”. In: *2015 European Radar Conference, EuRAD 2015 - Proceedings* (Dec. 2015), pp. 45–48. DOI: `10.1109/EURAD.2015.7346233`.

[22] W. Roberts et al. “Iterative adaptive approaches to MIMO radar imaging”. In: *IEEE Journal on Selected Topics in Signal Processing* 4.1 (Feb. 2010), pp. 5–20. DOI: `10.1109/JSTSP.2009.2038964`.

[23] P. Stoica, P. Babu, and J. Li. “New method of sparse parameter estimation in separable models and its use for spectral analysis of irregularly sampled data”. In: *IEEE Transactions on Signal Processing* 59.1 (2011), pp. 35–47. DOI: `10.1109/TSP.2010.2086452`.

[24] O. A. Krasnov et al. “PARSAX: High-resolution Doppler-polarimetric FMCW radar with dual-orthogonal signals”. In: *18-th INTERNATIONAL CONFERENCE ON MICROWAVES, RADAR AND WIRELESS COMMUNICATIONS*. 2010, pp. 1–5.

[25] Z. Li. *Design, Simulation and Validation of Dual-channel Polarimetric Agile Radar Technology*. 2011.

[26] R. J. Doviak and D. S. Zrnić. *Doppler radar and weather observations*. Academic Press, 1993, p. 562.

[27] O. A. Krasnov et al. “The PARSAX - full polarimetric FMCW radar with dual-orthogonal signals”. In: *2008 European Radar Conference*. 2008, pp. 84–87.

[28] D. S. Zrnic. “Spectral Moment Estimates from Correlated Pulse Pairs”. In: *IEEE Transactions on Aerospace and Electronic Systems* AES-13.4 (1977), pp. 344–354. DOI: `10.1109/TAES.1977.308467`.